PIV Measurements in Pumps

Dr. Detlev L. Wulff
TU Braunschweig
Institut für Strömungsmaschinen
Langer Kamp 6
D-38106 Braunschweig
GERMANY

d.wulff@tu-bs.de

ABSTRACT

Digital Particle Imaging Velocimetry (DPIV) is a powerful nonintrusive measuring technique that has become popular in the last decade with the availability of commercial systems. In contrast to Particle Image Velocimetry (PIV), which utilizes analogue imaging and therefore time-consuming post processing, for DPIV digital video recording is encountered which is ideally suited for digital data processing. This offers the advantage of near real-time velocity measurements and therefore eases application. The ability to measure instantaneous planar velocity fields makes it attractive for investigations of complex flow fields encountered in pumps. While standard systems allow measurement of two velocity components, stereo DPIV will deliver all three components in the measuring plane. This paper gives an overview on the basic principles of DPIV and the main components of standard systems. Special effort is made to report on the particularities of measurements in stationary as well as rotating components of pumps. The main topics of this report are:

- *Principles of DPIV*
- *Light sources, seeding and tracer particles, digital image recording*
- *Data processing*
- *Practical hints*
- *Optical access*
- *Refraction adaptation*
- *PIV-LIF*
- *Examples of DPIV measurements in pumps*

1.0 INTRODUCTION

Laser Radiation Hazard Warning.

In PIV systems powerful Nd:YAG lasers are employed which are classified as Class 4 radiation hazards. Please consult the laser safety instructions of your system before use.

Wulff, D.L. (2006) PIV Measurements in Pumps. In *Design and Analysis of High Speed Pumps* (pp. 5-1 – 5-36). Educational Notes RTO-EN-AVT-143, Paper 5. Neuilly-sur-Seine, France: RTO. Available from: http://www.rto.nato.int/abstracts.asp.

Report Documentation Page

Form Approved
OMB No. 0704-0188

1. REPORT DATE	2. REPORT TYPE	3. DATES COVERED
01 NOV 2006	**N/A**	**-**

4. TITLE AND SUBTITLE	5a. CONTRACT NUMBER
PIV Measurements in Pumps	5b. GRANT NUMBER
	5c. PROGRAM ELEMENT NUMBER
6. AUTHOR(S)	5d. PROJECT NUMBER
	5e. TASK NUMBER
	5f. WORK UNIT NUMBER
7. PERFORMING ORGANIZATION NAME(S) AND ADDRESS(ES) **TU Braunschweig Institut für Strömungsmaschinen Langer Kamp 6 D-38106 Braunschweig GERMANY**	8. PERFORMING ORGANIZATION REPORT NUMBER
9. SPONSORING/MONITORING AGENCY NAME(S) AND ADDRESS(ES)	10. SPONSOR/MONITOR'S ACRONYM(S)
	11. SPONSOR/MONITOR'S REPORT NUMBER(S)

12. DISTRIBUTION/AVAILABILITY STATEMENT
Approved for public release, distribution unlimited

13. SUPPLEMENTARY NOTES
See also ADM002051., The original document contains color images.

14. ABSTRACT

15. SUBJECT TERMS

16. SECURITY CLASSIFICATION OF:			17. LIMITATION OF ABSTRACT	18. NUMBER OF PAGES	19a. NAME OF RESPONSIBLE PERSON
a. REPORT	b. ABSTRACT	c. THIS PAGE			
unclassified	**unclassified**	**unclassified**	**UU**	**36**	

Velocity measurements of flow fields in pumps can be made by means of intrusive techniques like probes (e.g. pitot type, hydraulic, fast response, hot film) or by optical methods. Especially for measurements in rotating components intrusive techniques require special designed impellers and data transmission by means of telemetry. Therefore Laser Doppler Velocimetry (LDV) has been widely used for the last 30 years to investigate the flow field within rotating components of turbo machinery [20]. In contrast to PIV which delivers the whole velocity field from one measurement LDV allows only the measurement at a single point, however in most cases with high temporal resolution [15]. Since LDV measurements require a time consuming process of temporal and spatial averaging to improve the statistical confidence [20] in contrast DPIV can be regarded as a fast measuring technique. Planar measurement techniques offer significantly reduced data acquisition times over traditional point based measurement techniques and will therefore reduce facility testing time and cost [20]. One drawback of PIV is that it requires optical access for the light sheet as well as for the camera, which may sometimes be difficult to ensure. In these cases more traditional point based techniques like LDV and L2F [16] may be encountered. PIV and especially DPIV is a comparatively new method that has found its way from research laboratories to turnkey systems and we can now observe standardisation of PIV components as well as of measuring techniques. Consequently, this lecture is focused on the latter systems. For those who are more interested in PIV itself there are a lot of publications written by those who still develop PIV further.

2.0 PRINCIPLES OF DPIV

With Digital Particle Velocimetry (DPIV) the velocity of a flowing medium is measured by recording the displacement of small particles (= seeding) carried with the flow. According to Fig. 1 the seeded flow field is illuminated by two short laser pulses fired with a known time separation. Images of the illuminated particles are captured by a digital video camera placed perpendicular to the light sheet. The particle displacements in the flow field are found from the displacement in the image plane. Knowing the magnification and the time separation between the laser pulses, the velocity vector field on the measuring plane is found by:

$$c = \frac{\Delta x}{\Delta t}$$

where c = velocity [m/s]
Δx = displacement [m]
Δt = time between light pulses

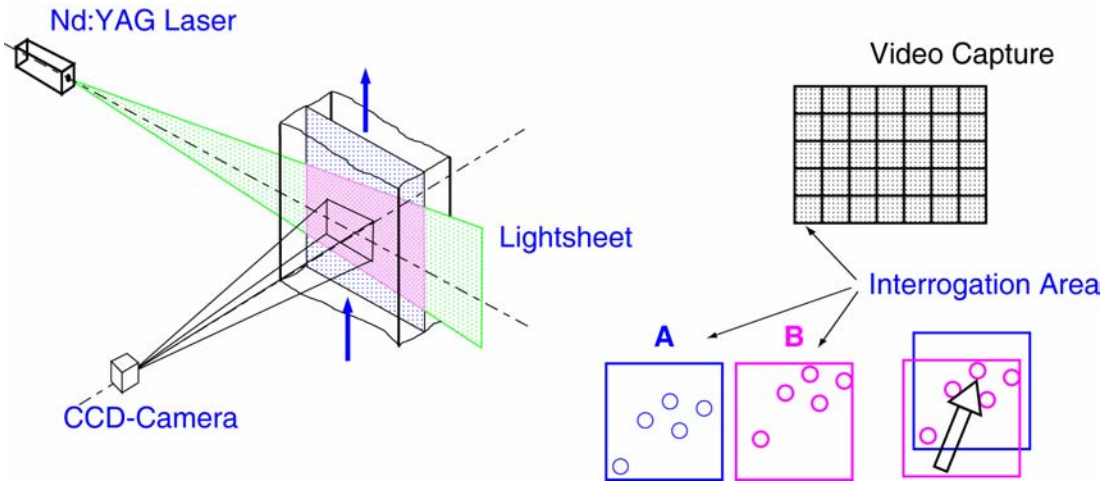

Figure 1: Arrangement for Particle Image Velocimetry in a Water Channel.

Since with PIV the displacement of particles and not of the flow itself is measured, it is essential that the seeding particles are able to follow the flow. Usually PIV is limited to velocity measurements, if accelerations are requested three or more subsequently recorded images would be necessary. The illuminated particles are recorded on different frames of the camera at two instants of time (in older systems two images have been recorded on the same frame). The camera images are divided in rectangular regions called interrogation areas. For example, typically size for an interrogation area is 32 x 32 or 64 x 64 pixels. The displacement of the particles within each pair (A, B in Fig. 1) of these interrogation areas is calculated by cross-correlation. Doing so for all interrogation areas will deliver the complete velocity field. With PIV it is not the velocity of a single particle measured (this is called Particle Tracking Velocimetry) but the average velocity of the particles within a finite interrogation area. It is therefore essential to ensure sufficient seeding in the whole flow field. A complete PIV experiment can be divided in the following four steps:

- Seeding the flow
- Illumination
- Image recording
- Post processing (analysis of the recordings)

While the principles of PIV are straightforward, a large number of investigations and technical progress has been necessary to develop the turn-key systems we have nowadays. But even today, the quality of the results achieved depends strongly on the skill of the operator.

2.1 Planar PIV (2C-2D)

Planar PIV delivers two velocity components in the measuring plane and is therefore also called 2C-2D PIV (2 components – 2 dimensions). This is the standard installation, where the camera position is perpendicular to the light sheet (Fig. 1). Since this configuration leads to least optical distortions it is the most straightforward set-up. It should be noted, that only the projection of the velocity vector into the light sheet plane is recorded; the out-of-plane component is lost, while the in-plane components are affected due to optical distortion and by decreasing signal-to-noise ration (SNR) due to loss of correlating particles, which are entering or leaving the light sheet between the recordings. To prevent this signal dropout, it is recommended [6] that the thickness of the light sheet should be adjusted to (Fig. 2):

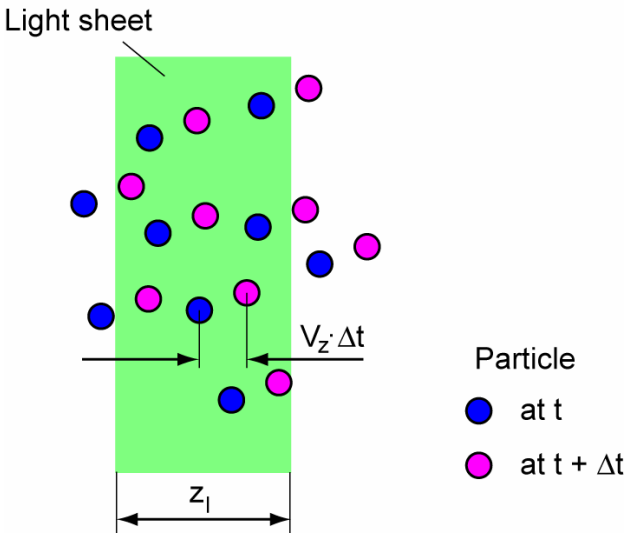

Figure 2: Out-of-Plane Velocity Determines Light Sheet Thickness.

$$\frac{v_z \Delta t}{z_l} \leq 0.25$$

where z_l = light sheet thickness
v_z = out-of-plane velocity component
Δt = time between the pulses

Even for a light sheet with properly adjusted thickness, the out-of-plane component will cause an error due to parallax effects (Fig. 3). Assume a seeding particle entering the light sheet at t and leaving t+Δt, if the particle moves along the camera axis, the in-plane component is measured correctly as zero but for all other positions it will introduce an error of the recorded in-plane component, which is proportional with the viewing angle. Since this effect is always present in 3D-flows, the use of long focal length lenses will help to minimize it. The problem can be cured completely by deployment of second camera, which will record the field of view from another angle.

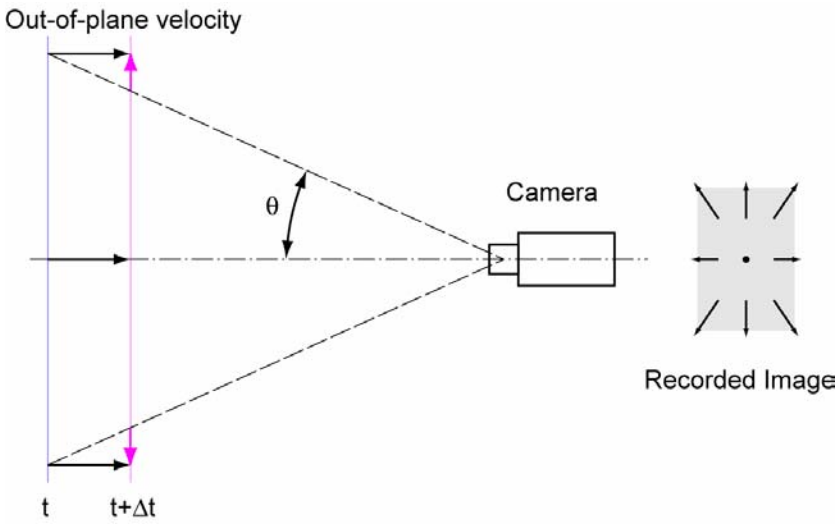

Figure 3: In-Plane Velocity Components are Affected by Out-of-Plane Components.

2.2 Stereo PIV 3C-2D

With a stereoscopic set-up (Fig. 4) it is possible to reconstruct all three velocity components in the measuring plane; it is therefore also called 3C-2D PIV (3 components, 2 dimensions). While it is possible to use two cameras perpendicular to the light sheet plane (translation method, e.g. [15]), mostly the angular displacement method is enabled, with both cameras axes tilted in respect to the measuring plane. This introduces two new problems: due to optical distortion, the scale factor is no longer constant, and the light sheet must remain within the focal depth. The magnification is determined in a preliminary calibration process, in which a target in the measuring plane is recorded with both cameras (Fig. 5). It should be noted that velocity measurements are limited to the area that is seen from both cameras.

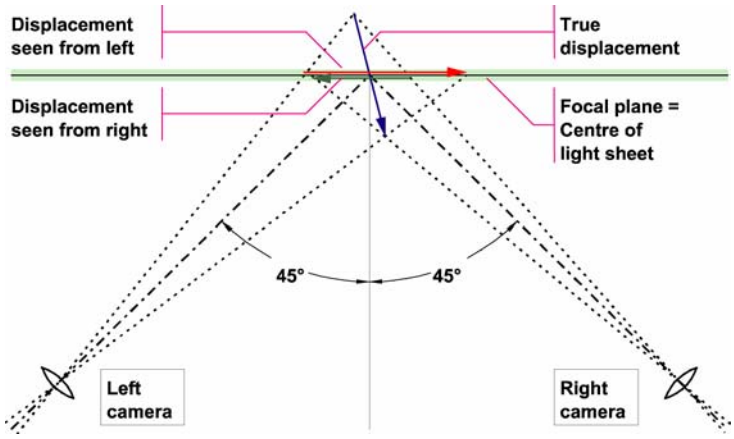

Figure 4: Stereo Imaging Configuration for Measurement of Three Velocity Components [6].

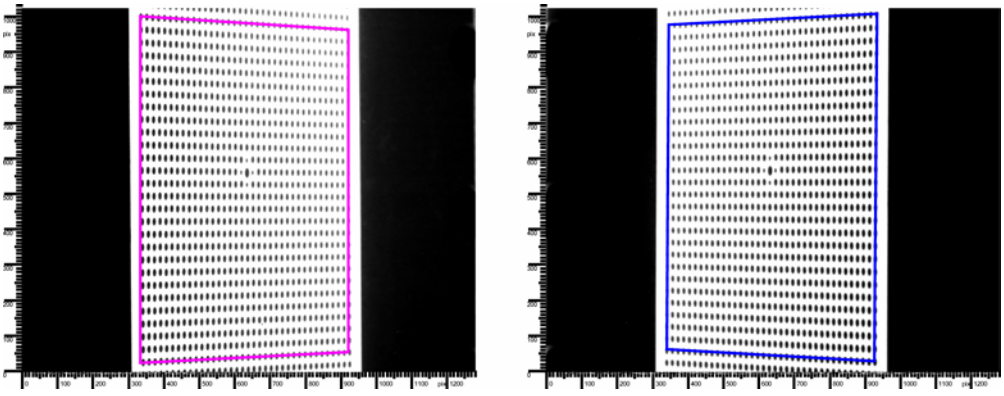

Figure 5: Images of Calibration Target (DANTEC®) Recorded by Left and Right Camera.

The measuring plane has to fall within the focal depth to ensure sharp images. The focal depth will increase with the lens stop number, that means closing the aperture. But this will cause a loss of light that must be compensated by more laser power. Therefore in stereoscopic PIV it is common practice to tilt the image plane to satisfy the SCHEIMPFLUG condition (Fig. 6), which demands that object plane, lens plane and image plane have a common point of intersection.

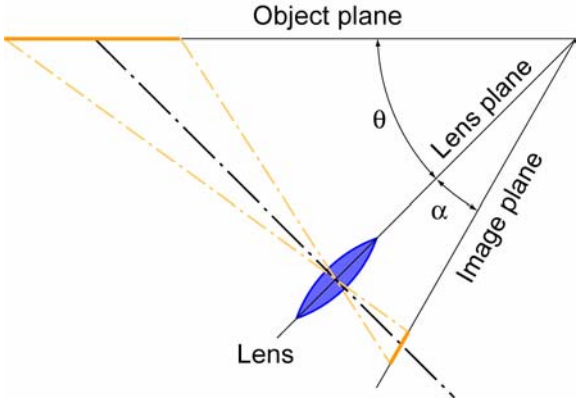

Figure 6: Scheimpflug Condition.

3.0 COMPONENTS

Fig. 7 illustrates the main components of a DPIV system. A pulsed laser is used as light source. Two 1-M-pixel cameras offer the option of 2C-2D as well as 3C-2D measurements, and e.g. the possibility of combined velocity measurement and cavitation observation. Fast data processing is ensured by means of two correlation boards, which allow near real-time velocity measurements. Heart of the system is the so called PIV processor which ensures data processing and timing of laser, camera and, if present, synchronisation with rotating machines.

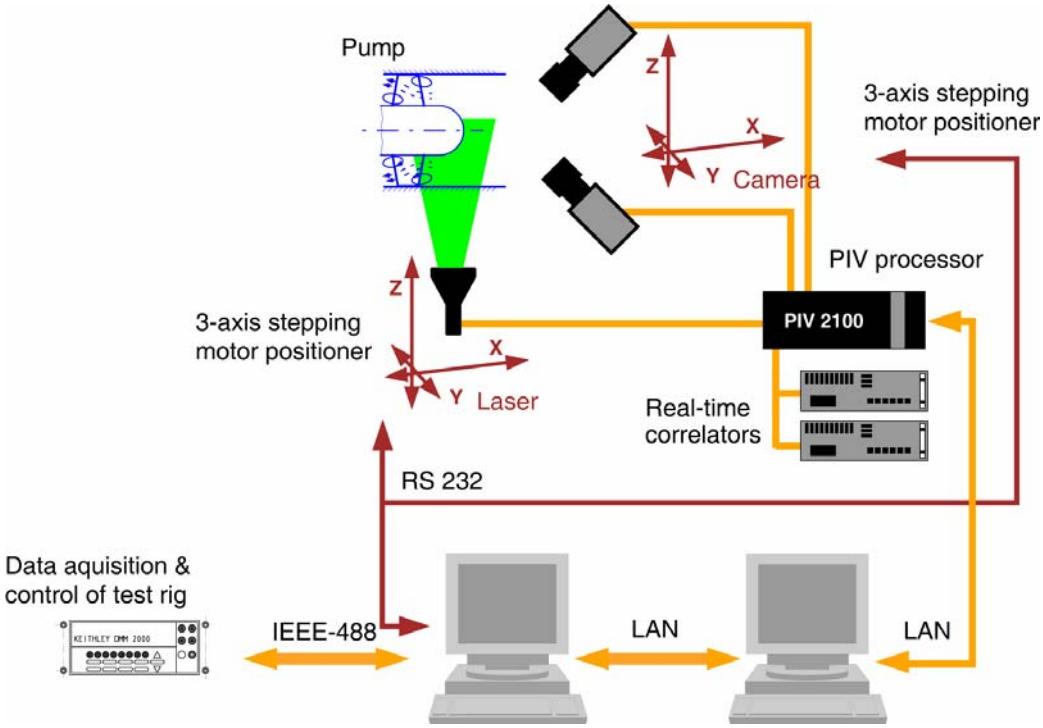

Figure 7: Main Components of DPIV-System.

A standard PC is used for controlling the PIV processor and data post processing. Cameras and laser head are mounted separately on two stepper motor controlled 3-axis positioners (Fig. 8). Controlling of the 3-axis positioner is done by a second PC, which is also used for controlling and data acquisition of the test circuit. As shown in chapter 5.3, for measurements in fluids with refraction indexes different from air it is necessary that laser and camera can be positioned independently. Fig. 9 shows a picture of a stereoscopic DPIV set-up at a pump test rig at Pfleiderer-Institute laboratory. Since the weight of a modern solid-state Nd:YAG laser head is low as 5 to 10 kg it is possible to mount it itself on a 3-axis-positioner. This eliminates the use of an articulated light guide arm which provides on one hand a safe coupling to the laser head but on the other hand there is a tendency of the laser beam to “wander” inside the arm as the arm is moved [20].

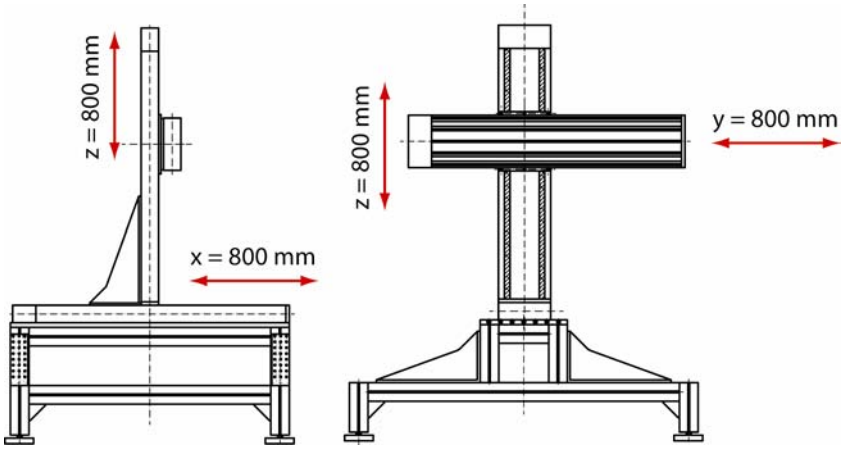

Figure 8: Stepper-Motor Controlled 3-Axis Positioner.

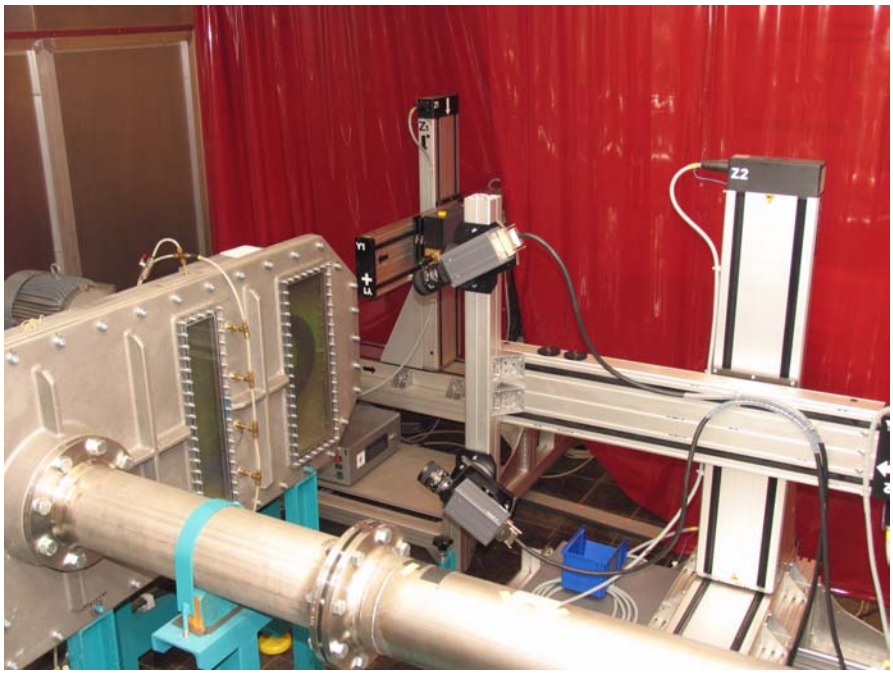

Figure 9: DPIV System with Stereo Imaging for Measurement of Three Velocity Components.

3.1 Light Sources

The common light source for DPIV is the pulsed double cavity Nd:YAG laser. Fig. 10 shows the schema of a double cavity Nd:YAG laser, which are in fact two lasers inserted into a housing, which contains the optics to combine the leaser beam path. Since Nd:YAG lasers emit infra-red radiation (λ = 1064 nm), the frequency is doubled to λ = 532 nm by means of a second harmonic generator into the visible (green) spectrum. In order to obtain short bursts of light energy and to control the energy of the laser beam, the lasing cavity is Q-switched. For example, the pulse width of the Nd:YAG laser from table 1 is short as 3 – 5 ns; multiplied with the rated energy of 100 mJ this will lead to an instantaneous power in the range of

$$P_{Pulse} = \frac{100 \cdot 10^{-3}}{(3...5) \cdot 10^{-9}} \frac{J}{s} = 20...33\,\mathrm{MW}$$

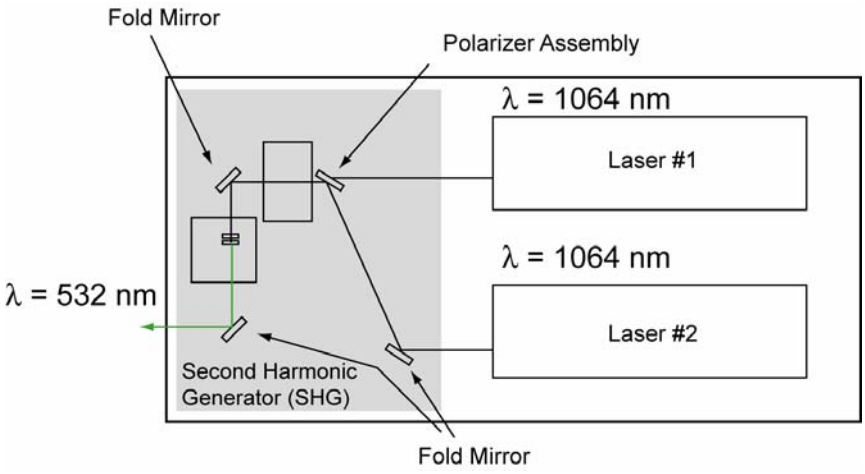

Figure 10: Layout of Gemini® PIV Nd:YAG Dual Laser Head (New Wave Research, Inc.).

Table 1: Specification of NewWave Gemini PIV Laser

Energy	2 x 100 mJ/pulse at 532 nm
Repetition Rate	15 Hz
Beam Diameter	4.5 mm
Pulse Width	3-5 ns
Relative Jitter	1 ns, with respect to external Trigger
Weight of Laser Head	7.3 kg
Power Supply	2 x 800 Watts

This example demonstrates why pulsed lasers are generally classified as a safety hazard. Even reflections of the laser beam may cause irreparable damages to human eyes and to CCD-cameras as well. The light sheet is generated by guiding the round laser beam through the light sheet optics. Depending on the application there are optics for different light sheet thickness, operation ranges and divergence angles available. The light sheet optics are mounted directly to the beam outlet of the laser head or if employed to the light guide system.

3.2 Seeding (Tracer Particles)

As mentioned already in PIV are not the velocities of the flow actually measured, but the velocities of particles suspended in the flow. It is therefore essential that seeding particles are small enough to track the flow accurately and on the other hand are big enough to scatter sufficient light for the camera to detect them. Ideally particles should have the same density like the fluid, which is investigated. In contrast to gases, in liquid flows this can satisfactorily be achieved as the data of seeding particles in table 2 show. Typically seeding particles for liquid flows are made from synthetic materials or from glass. From own experiments light scattering from silver coated hollow glass sphere is superior at the pay of slightly higher density.

Table 2: Specifications of Seeding Particles for Use in Liquid Flows [DANTEC®]

	Polyamide Seeding Particles	Hollow Glass Spheres	Silver Coated Hollow Glass Spheres	Fluorescent Polymer Particles
Mean diameter µm	5, 20, 50	10	10	10, 30, 75
Size distribution	1 – 10 µm 5 – 35 µm 30 – 70 µm	2 – 20 µm	2 – 20µm	1 – 20 µm 20 – 40 µm 50 – 100 µm
Particle shape	non-spherical but round	spherical	spherical	spherical
Density (g/cm³)	1.03	1.1	1.4	1.5
Melting point (°C)	175	740	740	250
Material	Polyamide 12	Borosilicate glass	Borosilicate glass	Melamine resin based polyester

3.3 Image Recording

3.3.1 Imaging

Since imaging is a photographic process some basic knowledge is necessary. According to Fig. 11 the following formulae and terms are commonly used to characterize imaging systems:

Lens formula $$\frac{1}{g}+\frac{1}{b}=\frac{1}{f}$$

Magnification $$M=\frac{b}{g}=\frac{B}{G}$$

Scale-Factor $$S=\frac{1}{M}=\frac{G}{B}$$

F-Number (lens stop) $$f_{\#}=\frac{f}{D}$$

where b = image distance
f = focal distance
g = object distance
D = aperture Diameter

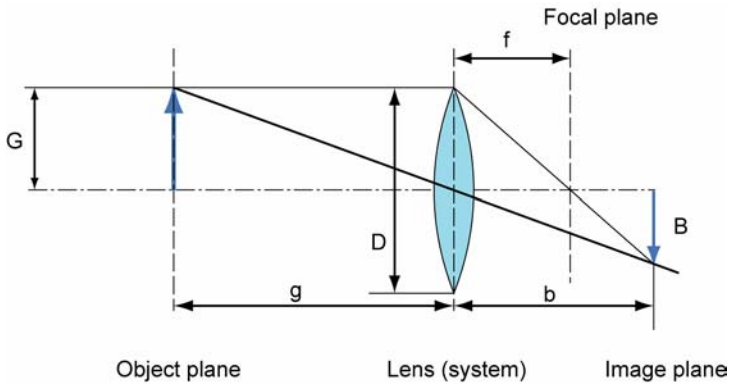

Figure 11: Imaging System.

The real break through for PIV was introduction of digital image recording, which is ideally suited for digital data processing. Common standard in DPIV today are special cross-correlation CCD (charge-coupled devices) cameras. Theses cameras are capable of recording two subsequent images on separate frames. Cross-correlation cameras heave generally a progressive scan interline chip layout (Fig. 12). Such chips comprise of light-sensitive cells and an equal number of storage cells. After recording the first image, the charges of the light-sensitive cells are transferred to the storage cells, while the second image is recorded. The data of the storage cells are sequentially transferred to the output shift register. The shortest delay between two recordings is approximately determined by the time, which is necessary to transfer the charges from the light sensitive cells to the storage cells. One disadvantage of progressive scan interline cameras is that storage cells occupy space on the CCD-chip which is therefore not light sensitive. The problem is diminished by adding an array of micro-lenses on front of the CCD-chip.

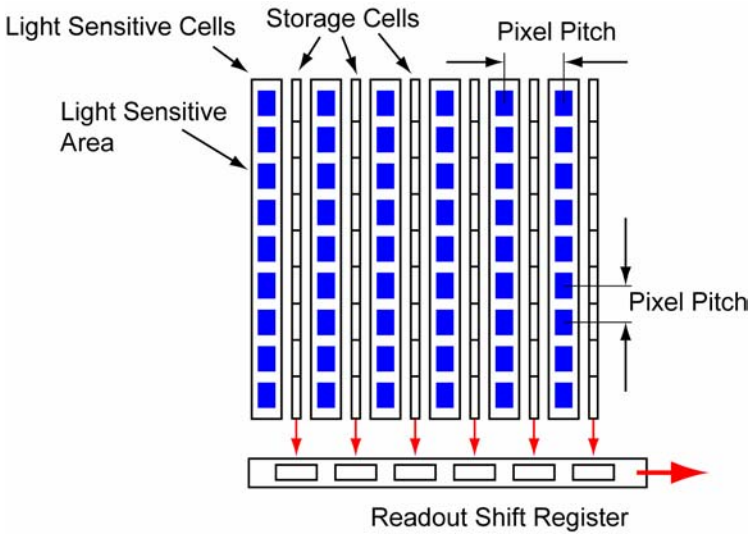

Figure 12: Progressive Scan Interline CCD Chip Layout.

The maximum frame rate of a CCD camera is determined by the time, which is needed to read out the data. Although the read-out time for the camera in Fig. 13 is 111 ms, the shortest time between two subsequent recordings is low as 0.2 µs (table 3). This is achieved by employing the so-called frame straddling technique [20]. The first image is recorded after triggering the camera, while the image of frame #1 is exposed by firing laser #1. The image data of frame #1 are then transferred to the storage cells and frame #2 is exposed by firing laser #2. Since reading out of the data from frame #1 takes for the given

example 111 ms frame #2 is exposed for the same time. It is therefore necessary to prevent firing the laser again during this time otherwise frame #2 would have been exposed twice. It is also recommended to perform DPIV measurements with low ambient light or best in dark to achieve two images with comparable exposure.

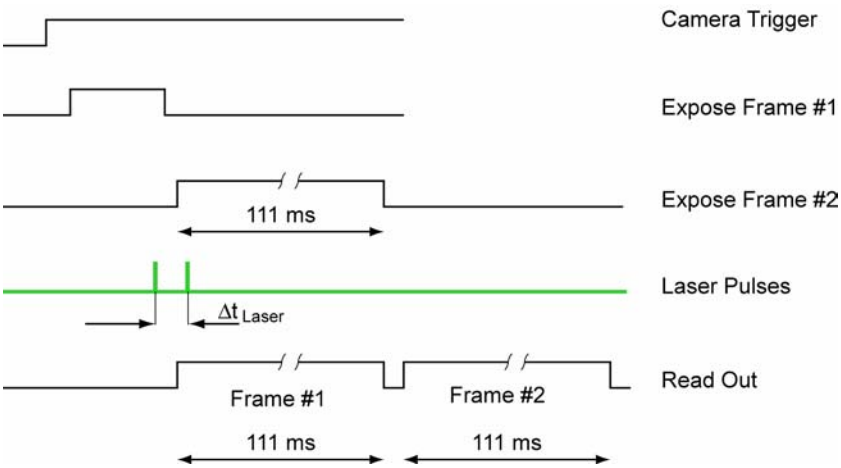

Figure 13: Timing Diagram for Double-Frame Camera and Frame Straddling Technique.

Table 3: Dantec® HiSensePIV/LIF Camera Specification

Mechanical	Cooling	Peltier/Convection to +5°C
Sensor	CCD type	Progressive scan interline
	Active pixels	1280 x 1024
	Pixel pitch	6.7 x 6.7 µm
	Active Area	8.6 x 6.9 mm
	Resolution	12 bit
Output	Max. frame rate	9 Hz
Cross-correlation	Pulse interval range	0.2 µs to 110 ms and n x 110 ms
	Double-frame rate	5 Hz

3.3.2 Diffraction

The image size of a seeding particle which is recorded by means of a camera is affected by diffraction on the aperture of the lenses and can therefore not directly calculated with the magnification-formula given above. The image of a distant point source does not appear as a point on the image plane but forms a Fraunhofer diffraction pattern even if it is imaged by perfect lenses [15]. Fig. 14 shows the intensity pattern of a point source in the image plane, this is known as Airy patterns. With decreasing aperture diameter – that means increasing lens stop numbers – the diameter of the Airy pattern increases. The image size of particle is given by [1], [15]

$$d_{\mathrm{Im}age} \approx \sqrt{\left(M \cdot d_p\right)^2 + d_{diff}^2} = \sqrt{\left(M \cdot d_p\right)^2 + \left(2.44 \cdot f_{\#} \cdot \lambda\left(M+1\right)\right)^2}$$

where d_p = diameter of the seeding particle

d_{diff} = diameter of Airy disk

$f_{\#}$ = lens stop number

λ = wavelength of the illuminating light source

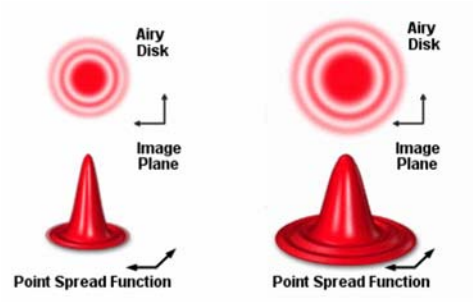

Figure 14: Airy Patterns for a Large (left) and a Smaller Aperture Diameter (right). [http://www.olympusmicro.com]

As an example, Fig. 15 shows the calculated image diameter for particles with 4 and 16 µm diameter. Obviously, the image diameter is affected by diffraction for scale factors below 10. As shown later, it is desirable that the size of a particle image is in the range of two to three pixels of the camera. Therefore the image diameter of particles in a PIV system are determined by

- Particle size
- Magnification
- Diffraction

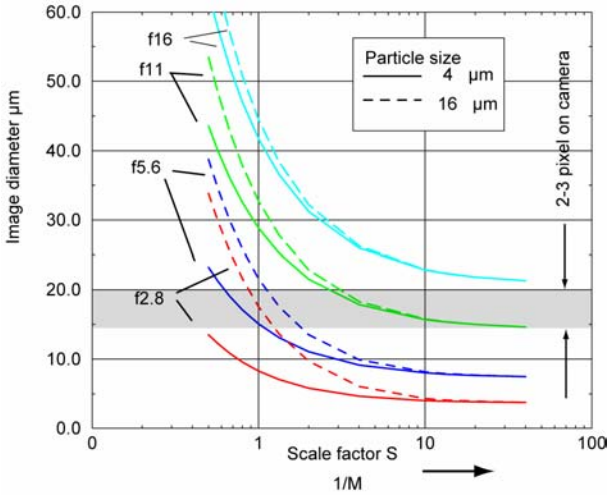

Figure 15: Aperture Stop (f-number) Affects Image Size of Small Particles.

4.0 PIV MEASUREMENTS

4.1 Image Evaluation by Means of Cross-Correlation

One major challenge in PIV is the displacement estimation from the recorded image pairs. Since for each pair of interrogation areas one average displacement vector is obtained, small interrogation areas will lead

to a high number of displacement vectors. Since the velocity vector in an interrogation area is a local average, it is recommended that the velocity variation within the flow field that is mapped by the interrogation area is less then 5-10 % to avoid zero-velocity biasing [6]. For reasons explained later the displacement should be limited to N/4 for an interrogation area with a side length of N. Drawback of high spatial resolution is the increase of uncertainty in estimating the displacement since smaller interrogation areas are employed. To utilise the full dynamic range it is necessary to adjust the time interval between the exposures that the maximum displacement is equal to N/4 pixel. In PIV therefore we have to compromise between

- Spatial resolution
- Velocity (displacement) resolution

There are several approaches to overcome the limitations mentioned above. By default the interrogation areas are located at the same position on both image frames. Imagine a flow field with a translation component of velocity, for example like the flow in a pipe. If the interrogation areas of the second frame are shifted to the average displacement, so that nearly every particle in interrogation area #1 corresponds to a particle in interrogation area #2, the loss of pairs is minimized and therefore a strong correlation is provided. Another benefit from shifting the second interrogation area is that sub-pixel approximation is improved which will lead to better velocity resolution. Another more advanced task is known as approximative interrogation. Approximation starts with comparatively large interrogation areas (e.g. 128x128 pixel) from which the mean displacements are estimated. The large interrogation areas are now divided into smaller ones, since their average displacements are known it is possible to shift the interrogation areas on frame #2 accordingly. Depending on the complexity of the flow field several steps of refinement may be necessary. This method is especially useful when measuring complex flows since it delivers good spatial resolution as well good dynamic range.

Fig. 16 shows one raw-data image and a pair of interrogation areas. The spatial shift given by a pair of interrogation areas may be described with a simple signal processing model [6], [15] as shown in Fig. 17.

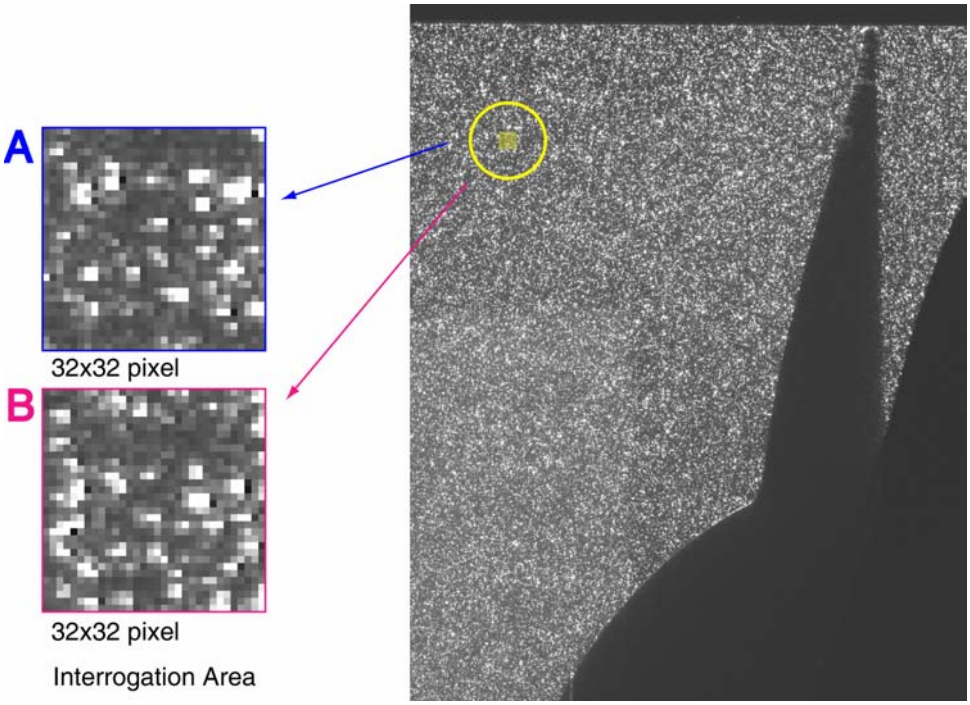

Figure 16: Raw-Data Image and Interrogation Area.

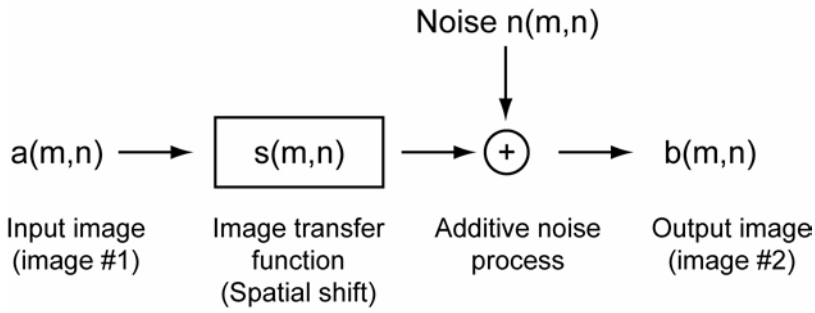

Figure 17: Image Displacement Function.

The functions a(m,n) and b(m,n) describe the light intensity within the interrogation area recorded at two instants of time. When a(m,n) is considered as input and b(m,n) as output, the image transfer function s(m,n) describes the spatial shift. The noise function n(m,n) is a result of seeding particles moving in or out of the interrogations areas in the period between the two recordings. The estimation of the displacement function s(m,n) is a statistical method of spatial cross-correlation. The discrete cross-correlation function $R_{ab}(m,n)$ of the sampled regions a(m,n) and b(m,n) is given by the expected value

$$R_{ab}(m,n) = E\left[a(m,n), b(m,n)\right]$$

$$R_{ab}(m,n) = \sum_{k=-U}^{k=U} \sum_{l=-V}^{k=V} a(k,l) \cdot b(k+m, l+n)$$

Fig. 18 demonstrates the calculated cross-correlation for the interrogation area shown in Fig. 16. The highest peak is observed when many particles match up with their corresponding shifted particles. Smaller correlation-peaks are observed when individual particles match with some other. The former is known as true correlation, while the latter is called random correlation. Seeding particles that are entering or leaving the interrogation area between the recordings, will not distribute to the true correlation because they are missing one of the images. They do however distribute to random correlation and increase therefore the signal-to-noise ratio. In PIV this phenomenon is known as “loss-of-pairs” or “signal-drop-out”. One should aware that the cross-correlation process always will deliver results, if they are meaningful or not. The time-consuming calculation of the cross-correlation function can be shortened by using the Fast Fourier Transformation (FFT). It yields generally

Time Domain $\Leftrightarrow$ Frequency Domain

$$x(t) \Leftrightarrow X(\omega)$$
$$y(t) \Leftrightarrow Y(\omega)$$
$$R_{xy}(t) = x(t) \times y(t) \Leftrightarrow \Phi_{xy} = X(\omega) \cdot Y^{*}(\omega)$$

where

$x(t)$, $y(t)$	= signal in the time or space domain
$X(t)$, $Y(t)$	= signal in the frequency domain
$R_{xy}(t)$	= cross-correlation function
$\Phi_{xy}(\omega)$	= power spectral density
$Y^{*}(\omega)$	= conjugated complex of $Y(\omega)$

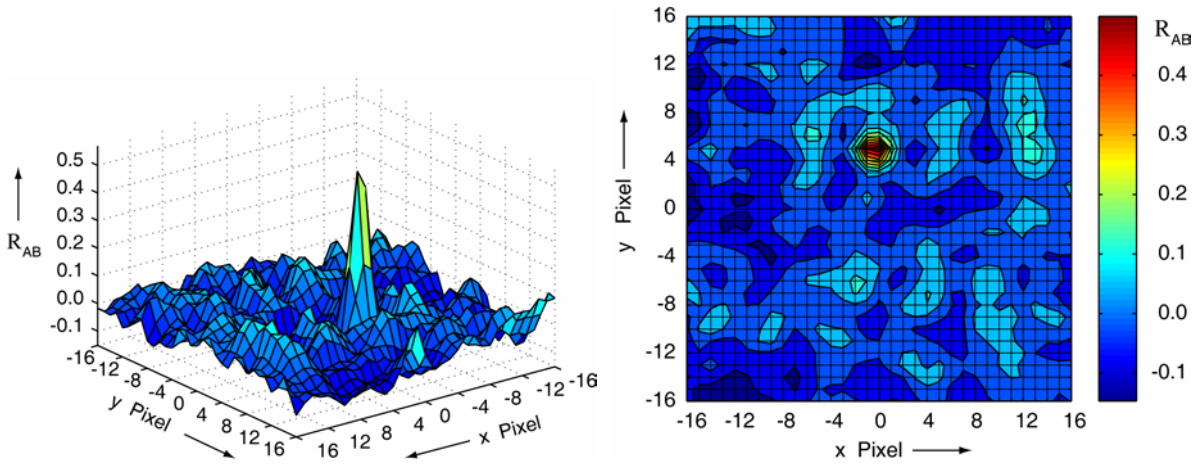

Figure 18: Cross-Correlation for One Interrogation Area of 32x32 Pixels.

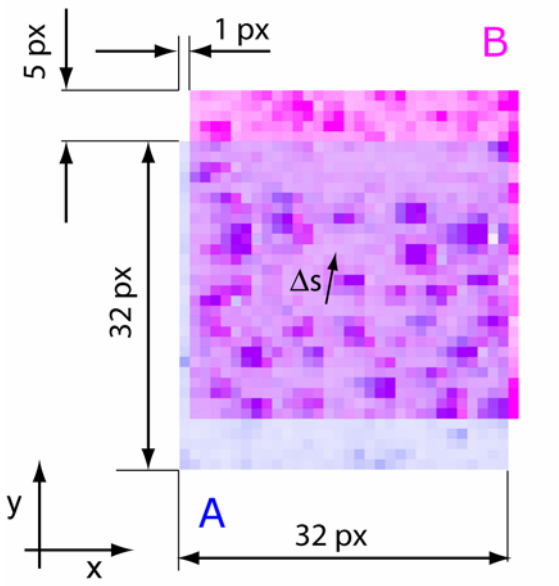

Figure 19: Interrogation Areas at Estimated Displacement.

Fig. 20 shows the flowchart for performing cross-calculation by means of fast Fourier transforms. This method is broadly used in DPIV to speed up the correlation process. The fast Fourier transform assumes the sampled regions to be periodic in space, and generates therefore a circular form of the cross-correlation which does not fall off to zero at the edges as with the linear technique. Hence an increase in background noise will be noted especially near the edges of the interrogation areas. Another consequence of employing the fast Fourier method is that we have to respect the Nyquist (or Shannon) sampling theorem that limits the maximum recoverable spatial displacement to half of the window (= interrogation area) size. For example, the maximum displacement for a given window length of N pixels is therefore N/2, otherwise the correlation peak will be folded back into the interrogation area and cause change of sign of the measured velocities [15]. Since the signal-to-noise ratio increase with increasing spatial shift, it is recommended to limit the spatial shift to N/4. There are several approaches to increase the signal-to-noise ratio by means of data windowing but these introduce other problems, which had to be solved [15]. The signal-to-noise ratio is strongly affected by number of seeding particles within the interrogation area. Generally, a minimum of 5 particles/region is recommended to achieve meaningful results [19].

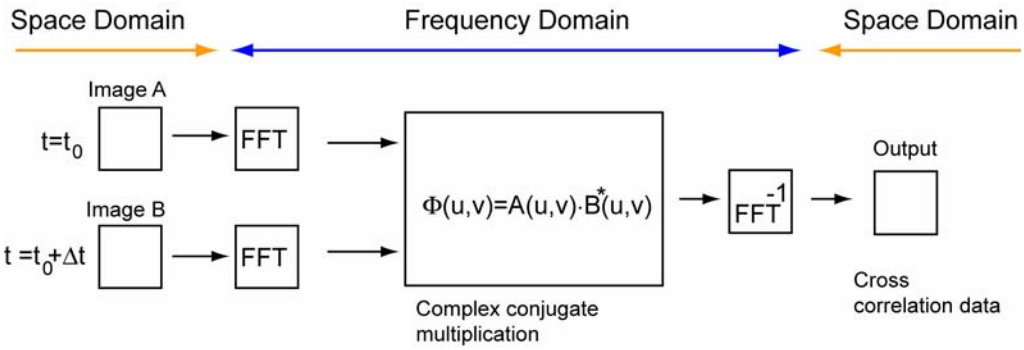

Figure 20: Cross-Correlation Employing Fast Fourier Transforms.

In Fig. 21 slices in x and y-direction through the correlation peak from Fig. 18 are shown. Since the input data itself is discretised, the correlation values exist only for integral shifts. With the above mentioned limitation of N/4 pixel shift, an interrogation area of N=32 pixel would be limited to 8 velocity classes with an uncertainty of ±1/2 pixel. The resolution can be improved in the range from 1/20 of a pixel [15] for 8-bit cameras up to 1/64 for 12-bit cameras [6] when employing sub-pixel interpolation by means of three-point estimators (Fig. 21). However, there is a tendency that data are biased to integer pixel values, which is also known as pixel locking. For example, the histogram in Fig. 22 shows a strong pixel-locking effect, instead of the expected "gaussian" velocity distribution. To get best results from sub-pixel interpolation it is recommended that the image size of particles is in the range from 2 to 3 pixels [15], [6], which in turn lead to well shaped cross-correlation peaks that will minimize pixel-locking. One common trick to broaden the correlation-peak is therefore slightly defocusing the lens to achieved blurred images. Another way is using filters as shown in Fig. 23, which will also help to improve the image data.

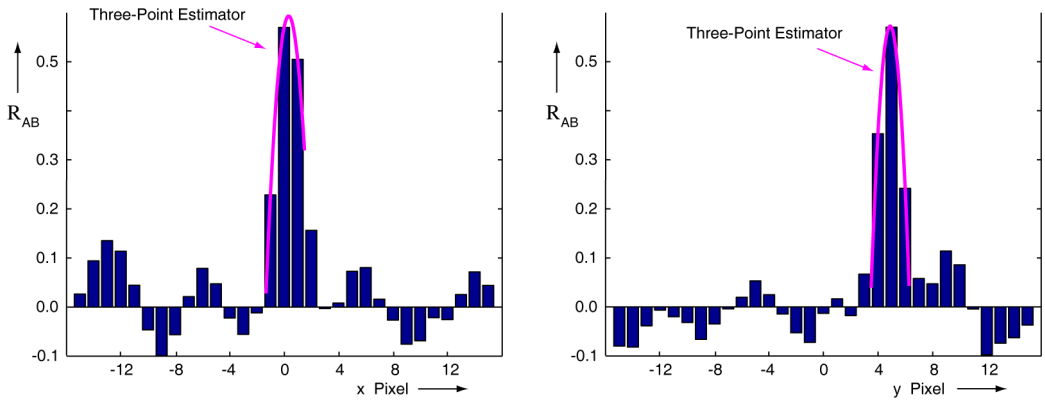

Figure 21: Sub-Pixel Approximation by Means of Three-Point Estimators.

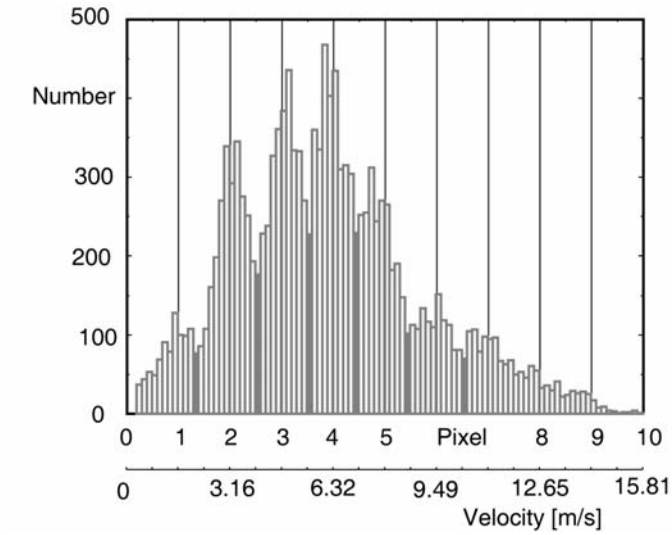

Figure 22: Histogram of Measured Velocities (Pixel Locking).

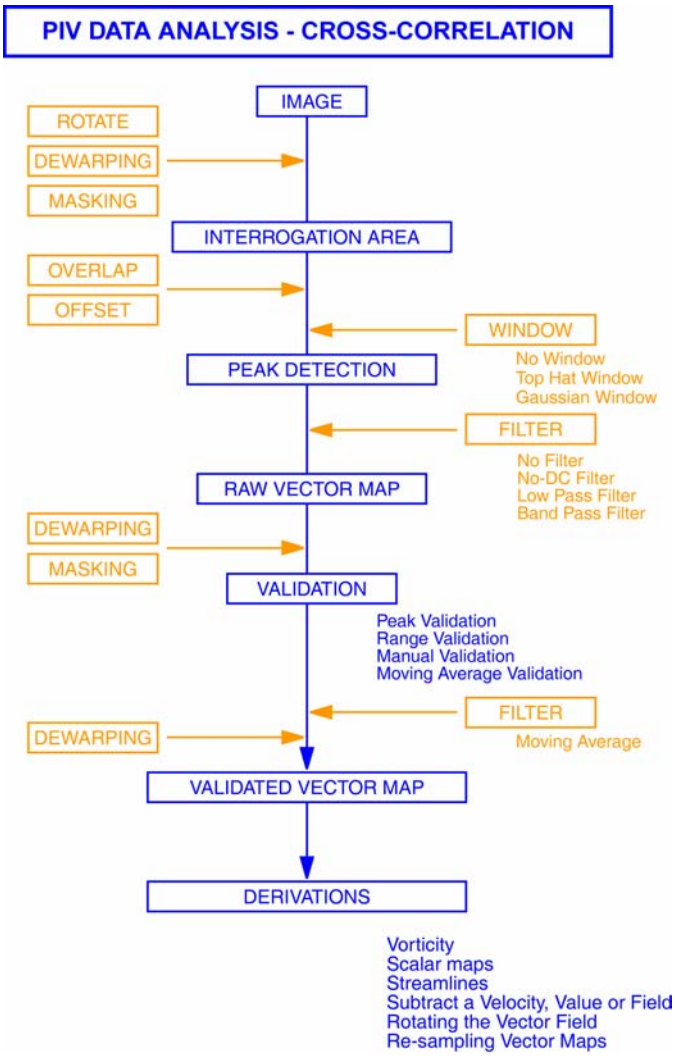

Figure 23: Flow Chart of DPIV Data Processing.

4.2 Post-Processing of PIV Data (Data Processing)

Outcome of the cross-correlation process is vector map, with one velocity vector for each interrogation area. As mentioned, cross-correlation will always deliver an outcome weather the input is meaningful or not. Therefore the vector map is also called raw-vector map and it is necessary to validate the vector map. There are several reasons, which may lead to invalid (spurious) vectors. Since in PIV the complete flow field at an instant time is measured, there may be regions in which the seeding are not sufficient or, for example, air bubbles in water will cause strong reflections. Reflections from walls or windows or even minor scratches on the window itself will cause disturbances. Fig. 23 shows a flow chart of DPIV data processing and validation. This process will be explained with the data of a pump impeller given in Fig. 24. Measuring section is near inlet of the impeller (Fig. 24 a)). While impeller blades made from Plexiglas ensure illuminating. The yellow grid marks the interrogation area size of 32x32 pixel. All regions of the image that do not belong to the flow field or shall not be investigated have to be “removed”, that means they have to be masked. This is shown in Fig. 24 b) where these regions are masked with green colour. Outcome of the cross-correlation process is a raw-vector map, which is given in Fig. 24 c). The vector number is higher than number of interrogation areas since cross-correlation is performed with 25% overlapping. Blue vectors indicate the measured flow, while red vectors indicate masked areas. To ease the understanding, the circumferential speed of the impeller has been subtracted from all measured velocities to achieve relative velocities. Obviously there are several spurious vectors; most of them are caused by imperfection in the recorded image itself. For example, in Fig. 24 a) it is observed that the light sheet intensity decreases near the right side of the image, which will lead to less scattering of the particles and in turn to a loss of information.

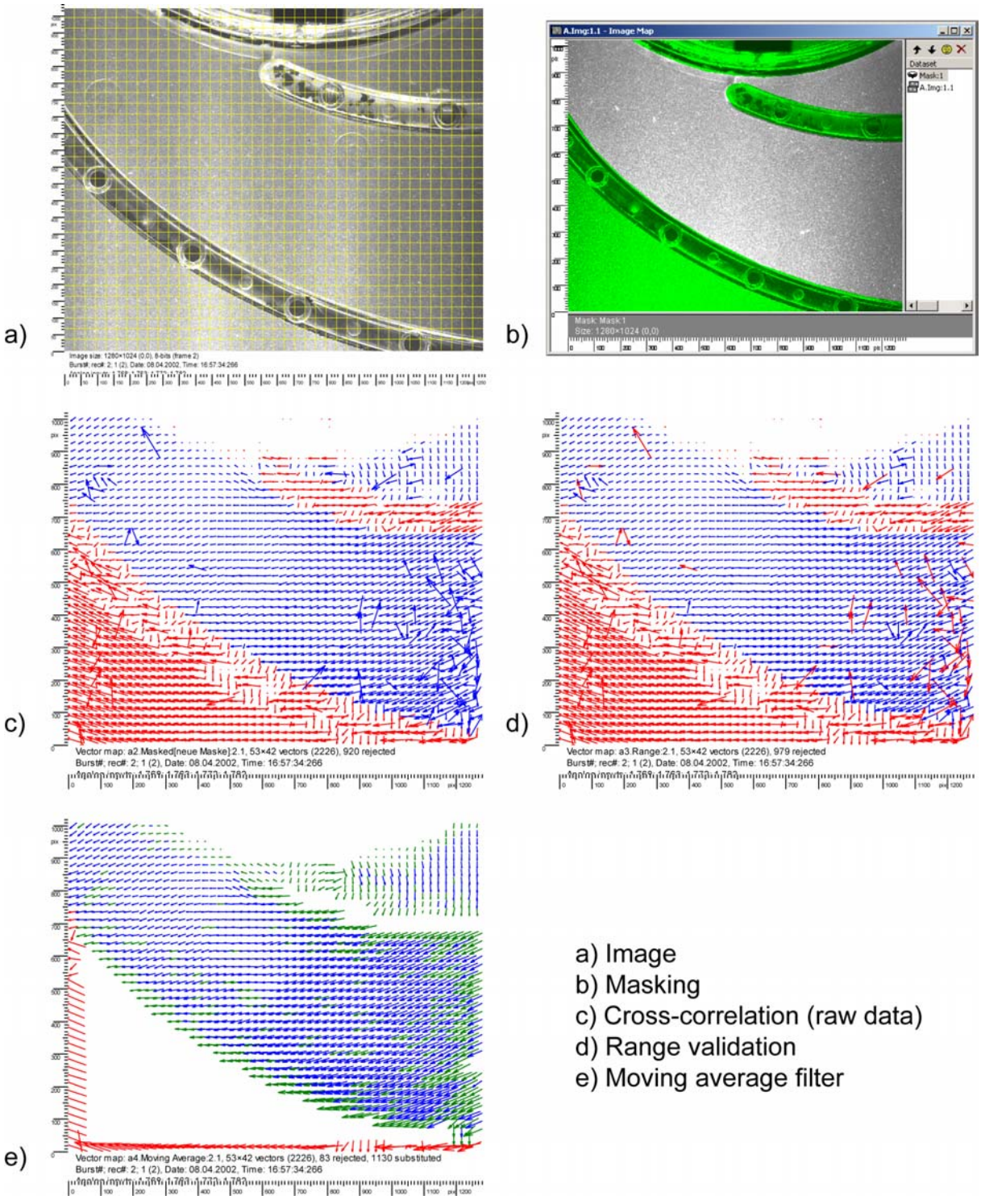

Figure 24: Post Processing of PIV Data.

Even weak reflections, for example as observed on screws in the back plane of impeller causes spurious vectors indicating the impeller velocity and not that of the flow. With some effort the aforementioned problems may be lowered, but a completely valid raw-data map will seldom be processed. The next step is validating the raw-data; in this case a range validation was performed. All vectors over a given limit were marked as invalid, these are also marked with red colour in Fig. 24 d). In a last step a moving average

filter is applied to smoothen the vector field. All substituted vectors are indicated by green colour (Fig. 24e).

5.0 PIV MEASUREMENTS IN PUMPS

5.1 PIV in Rotating Components

As an optical measurement method PIV allows the measurement in rotating components of fluid machinery, provided that optical access for laser beam and camera exist. As mentioned already timing is a sophisticated task in DPIV (Fig. 13) and this is especially true when measuring in rotating machines. Without synchronization with the rotating machine it would be possible to perform measurements, but the impeller position recorded would be stochastic. To perform phase averaged measurements with rotating machines there is a one-per-revolution trigger signal necessary, which is lead to the timing board of PIV system. Since a Nd:YAG laser must be kept pulsing continuously to maintain thermal balance within the laser cavity, measurements are only possible, when the trigger generated from the rotating machine falls into a time window within the laser pulse cycle. This method is therefore also called window trigger mode. By adding a time delay to the trigger signal from the rotating machine, the measured impeller position can be adjusted. Despite DPIV is a method, which is capable for measuring instantaneous velocity fields, in many cases also phase averaged values are requested. To achieve that, a synchronization method with low jitter is necessary.

5.2 Practical Hints

5.2.1 Equability of Laser Beams

For cross-correlation it is essential that both recorded images deliver comparable information, therefore both images should have the same exposition. To achieve this, the energy of the two laser pulses must be equal. This should be checked by means of a laser energy meter. The main components of an energy meter are a pyroelectric sensor on which the laser beam is fired and a special voltmeter to indicate the metered energy (Fig. 25). Some energy meters also deliver further useful information, for example, statistics on the energy of the recorded pulses. With the measured data as shown in Fig. 26, equal energy for both pulses is achieved by selecting the appropriate Q-switch delay.

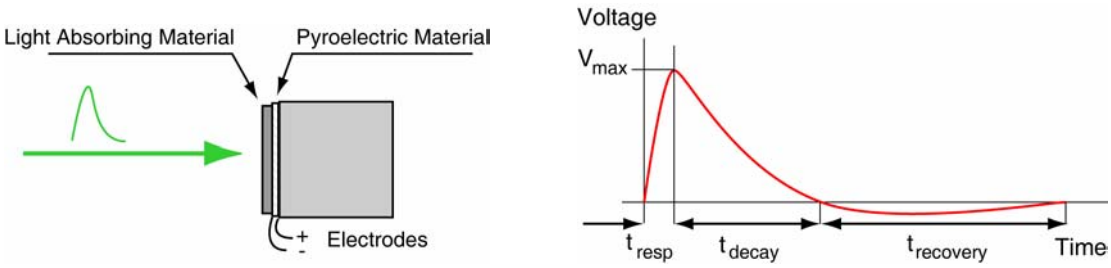

Figure 25: Schema of Laser Energy Meter and its Response Characteristics [GENTEC®].

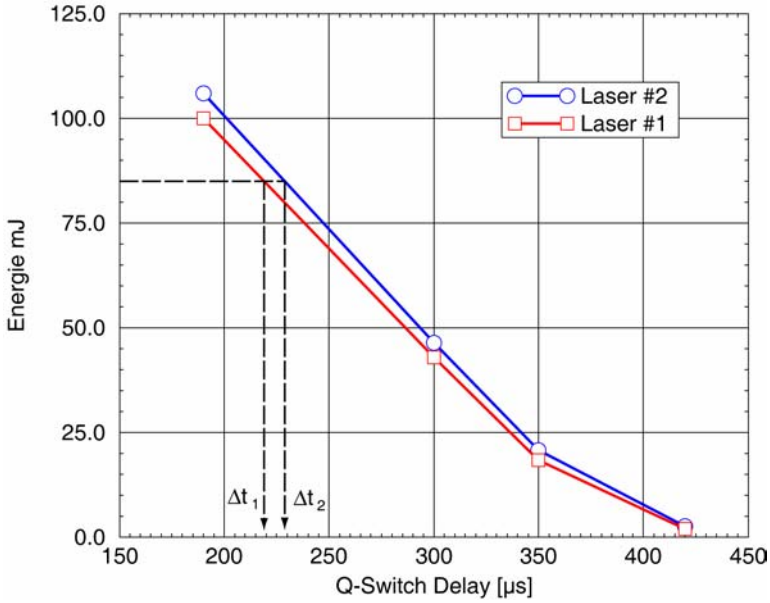

Figure 26: Equability of Laser Beams is Assured by Adjusting the Q-Switch Delays.

5.2.2 Alignment of Laser Beams

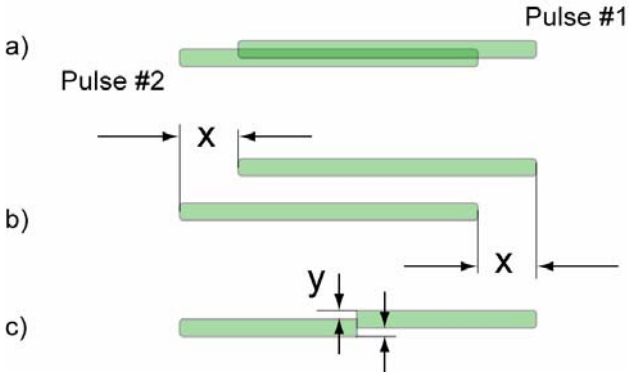

Figure 27: Images of Misaligned Light Sheets.

In a double cavity laser are in fact two lasers employed, the temporally separated pulses must overlap each other to produce the best signal in PIV. Slightly misaligned light sheets will increase the signal-to-noise ratio, while light sheets that do not overlap each other will deliver two images without any valid correlation particles. Since for adjustment the laser must be operated with open cover, one should be aware of radiation. To check the overlap of the two beams it is best to fire the laser on a photographic paper to register the light sheets images. It is best to cover half of the photographic paper, fire laser #1 and then cover the other half of the paper and fire laser #2. Fig. 28 shows the traces for different states of alignment.

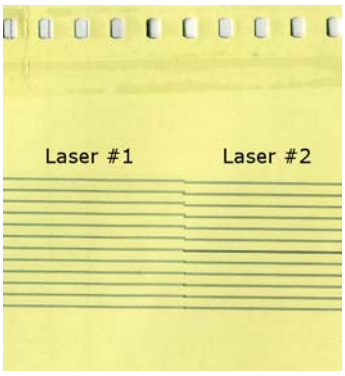

Figure 28: Light Sheet Traces on Photographic Paper for Different States of Alignment.

5.3 Optical Access

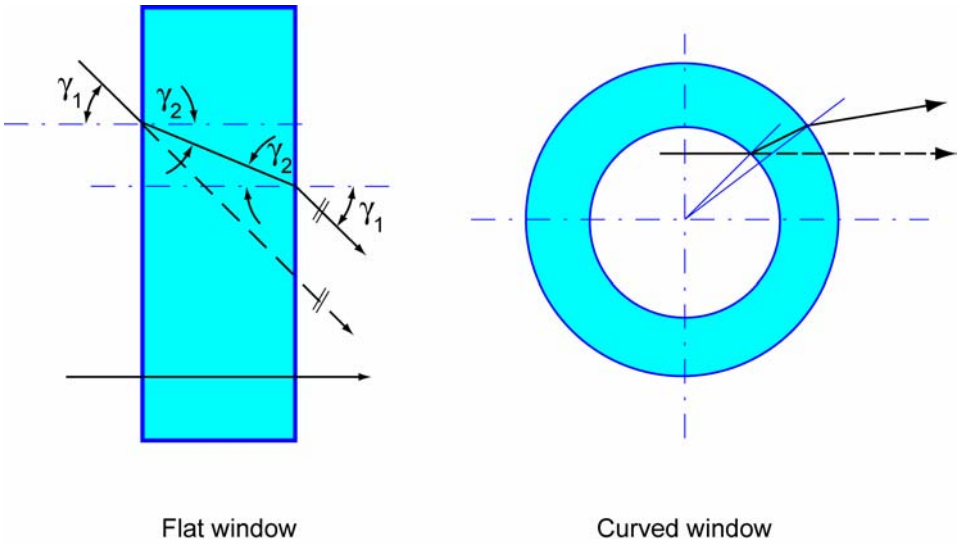

Figure 29: While Flat Window Leads only to Parallel Translation, a Curved Window Causes Optical Distortion.

For PIV measurements in pumps we need windows for the laser beam as well as for image recording. Plexiglas (perspex) is commonly used as material for windows, because of its good optical properties and ease to be machined in several ways. Since the optical density from Plexiglas is different from air, there will occur refraction of a light beam when entering or leaving the window. According to SNELLIUS law it yields

$$\frac{\sin\gamma_1}{\sin\gamma_2} = \frac{n_2}{n_1} = \frac{c_1}{c_2}$$

where γ = angle, measured perpendicular to separation plane
n = refraction index
c = velocity of light

Table 4: Refraction Indexes

Water/Air	n = 1.333
Plexiglas/Air	n = 1.491
Plexiglas/Water	n = 1.119

As long as flat windows are employed this will only a cause a parallel translation of the light beams and therefore be the best choise if possible. All curved surfaces will lead to more or less optical distortion, which will increase with wall thickness and curvature. In most cases we use water as fluid in pumps and we must take the additional refraction in account. Since curved windows cannot be omitted, there are several approaches to overcome the problem; some of them are shown in Fig. 30. There is the idea of enclosing the test section in a container with flat windows, which is filled with the same fluid as the test section. Minimizing the thickness of the test sections wall will minimize the distortion as well. If a “flat” test section (Fig. 30, right) is employed with the camera viewing perpendicular to the flat walls, the refraction caused by curved walls will be limited to the light sheet itself. This will lead to a non-uniform light distribution, which may often be accepted.

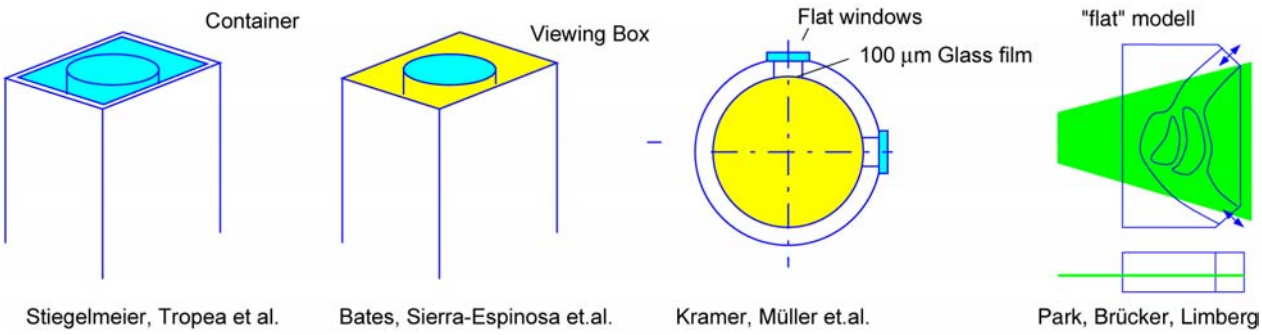

Figure 30: Different Approaches to Minimize Optical Distortion.

Like Fig. 31 shows, due to refraction an object in a liquid seems to be nearer than it is. This can easily be observed when watching objects under water. With PIV the flow field is often investigated by moving the light sheet and therefore the image plane to different immersion depth. To keep the recorded image in focus also the camera has to be moved, but not on the same amount as the laser. From Fig. 31 it follows

$$\Delta x_{Laser} = \Delta x_{Camera} \cdot \frac{\tan \gamma_1}{\tan \gamma_2}$$

Since in DPIV it is advisable to use small aperture angles, the equation above can often be simplified to

$$\Delta x_{Laser} \approx \Delta x_{Camera} \cdot \frac{\sin \gamma_1}{\sin \gamma_2} = \Delta x_{Camera} \cdot \frac{n_2}{n_1}$$

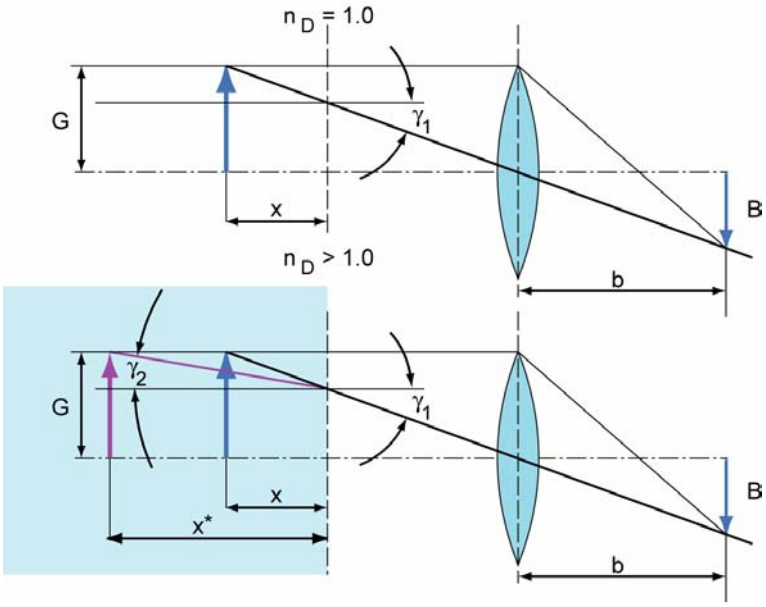

Figure 31: Refraction has to be Considered to Keep Image Focus Constant.

For a common set-up as shown in Fig. 32, the light sheet determines the measuring plane and the image is recorded with a camera through a plan Plexiglas window. If the light sheet for example is moved by Δx_{Laser} from position 1 to position 2, the camera has to been moved only the smaller distance of Δx_{Camera} to keep the image in focus. This is the reason why laser and camera must be positioned independently when performing PIV measurements in water.

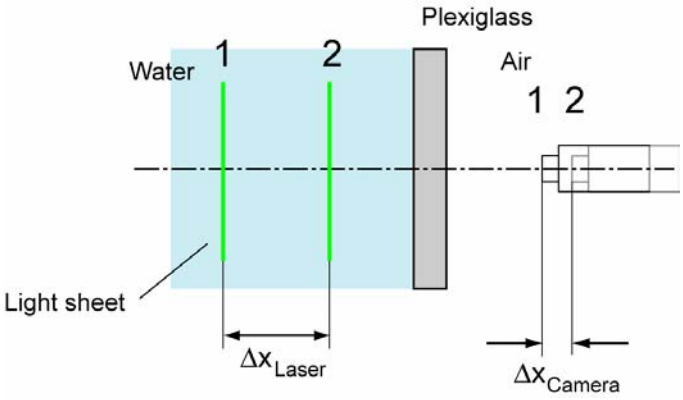

Figure 32: Different Traverse Paths for Light Sheet and Camera are Necessary to Keep in Focus.

5.4 Refraction Adaptation

The problem with distortion caused by refraction on curved walls can completely overcome by fully matching the refractive indexes of working fluid with the window glass. If Plexiglas windows are enabled for example, the refraction index of the working fluid must be according to table 4 n = 1.491. There are several working fluids, which have been used for matching the refractive indexes:

Table 5: Examples of Working Fluids Used for Refraction Adaptation

Working Fluid	Remarks	References
Mixing of two diesel oils		Stiegelmeier et. al. [17]
64% solution of sodium iodide in water	+ kin. viscosity 1.1×10^{-6} m^2/s - difficult to handle	Chow et. al. [5]
Naphthenic process oils	- kin. viscosity 1.2×10^{-5} m^2/s + easy to handle	Brunn, Nitsche [4]

At Pfleiderer-Institute laboratory we have made some DPIV measurements in an axial flow pump using naphtenic process oil for refraction adaptation. Fig. 33 shows the refraction indexes versus temperature for different SHELL® fabrication oils. At a temperature of ca. 23°C the refraction index of the chosen oil SHELL GRAVEX 917 matches with that of Plexiglas. As illustrated in Fig. 34, when using the matched working fluid there is no refraction on the circular wall, theses walls are actually invisible. To keep the refraction index in the desired range, the test rig is equipped with a heat exchanger. Main drawback of using fabrication oils is the increase in viscosity, which is according to Fig. 33 at least 10 times higher. It should also be mentioned that the electric conductivity is very low, so that electro magnetic flow meters cannot be used to measure the volume flow in the test rig.

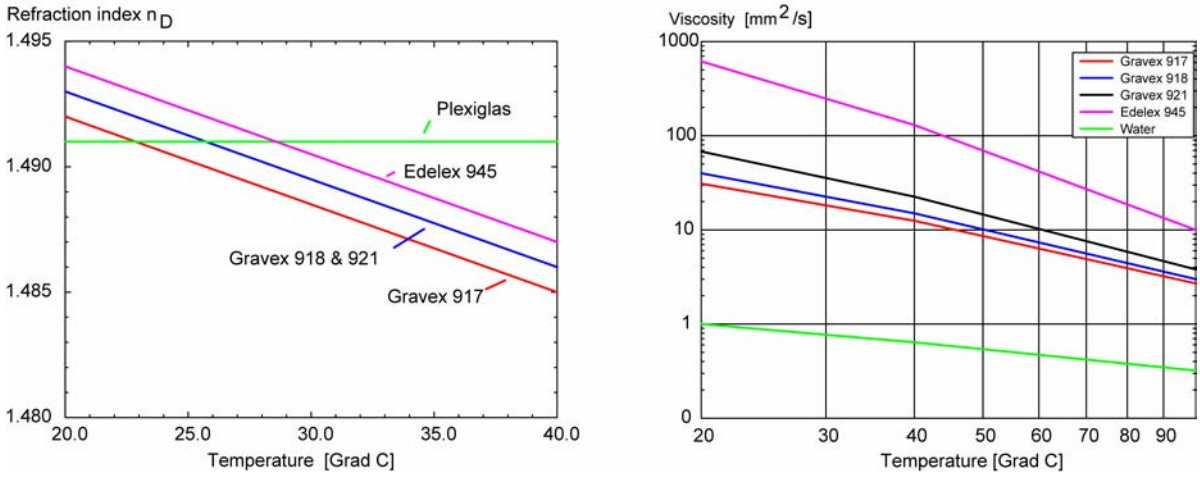

Figure 33: Refraction Index (left) and Viscosity (right) versus Temperature for SHELL Fabrication Oils.

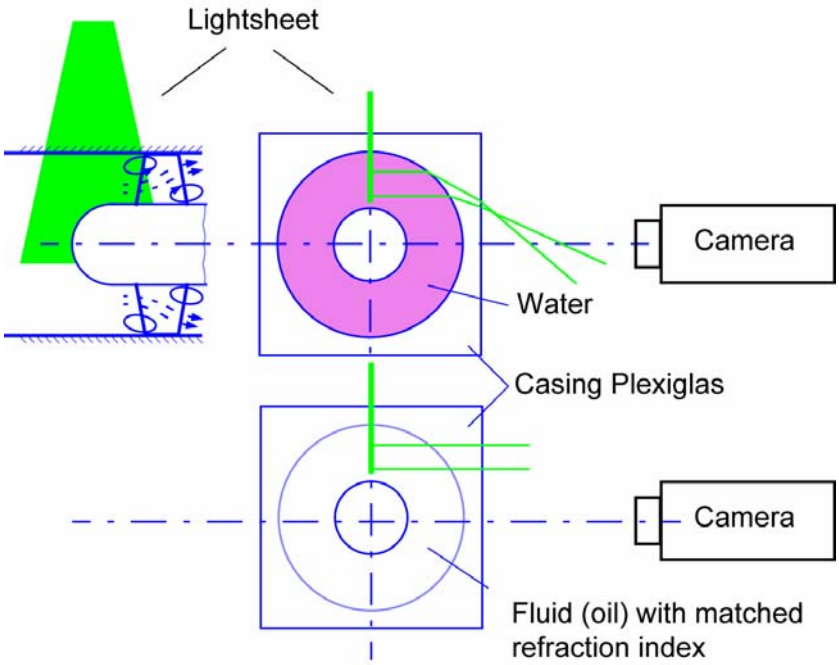

Figure 34: Refraction Adaptation Allows Measurements in Complex Geometries.

5.5 PIV-LIF

The common light source for PIV is an Nd:Yag laser with a wavelength of $\lambda = 532$ nm which is observed as green light. When standard seeding particles are illuminated by a green light sheet they will scatter light of same colour back. There are also fluorescent particles (see table 2) available which scatter orange light when they are illuminated by green laser light. This is called laser-induced fluorescence (LIF) and in connection with PIV it is also known as PIV-LIF. To achieve fluorescence the seeding particles are coloured with Rhodamine. To get benefit with PIV from LIF it is necessary to employ optical filters with the cameras.

According to Fig. 35 two filters are commonly used, a band pass filter for the green scattered light and a low pass filter for the orange light. The band pass filter may also be employed for standard PIV measurements, since it reduces ambient light on the recorded images. When measurements with laser-induced fluorescence are performed and the camera is equipped with the low pass filter, only the orange scattered light is recorded. Since all unwanted reflection from walls or windows are in green light, they cannot pass the filter and therefore not obstruct the recorded image. This is a very efficient method to increase the signal-to-noise ratio. *Pedersen* [14] made comprehensive measurements in a Plexiglas pump with this technique. Another approach for PIV-LIF is the measurement of two-phase flows, for example air/water or cavitation/water. The velocity of the water is recorded with the first camera, which is equipped with the low pass filter to detect the orange particles, while the second camera with the band pass filter will detect the cavitation or gas bubbles.

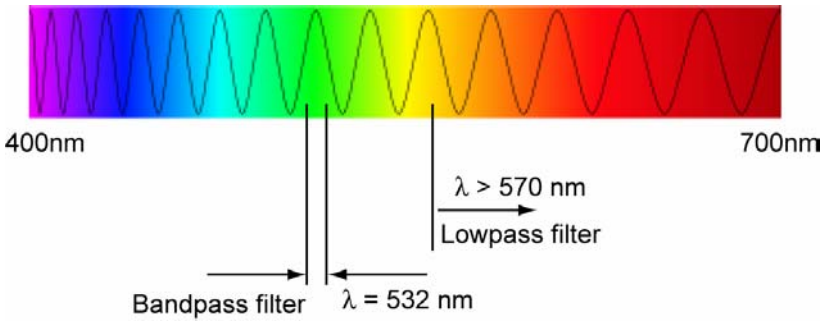

Figure 35: Band Pass and Low Pass Filter for Use with PIV-LIF.

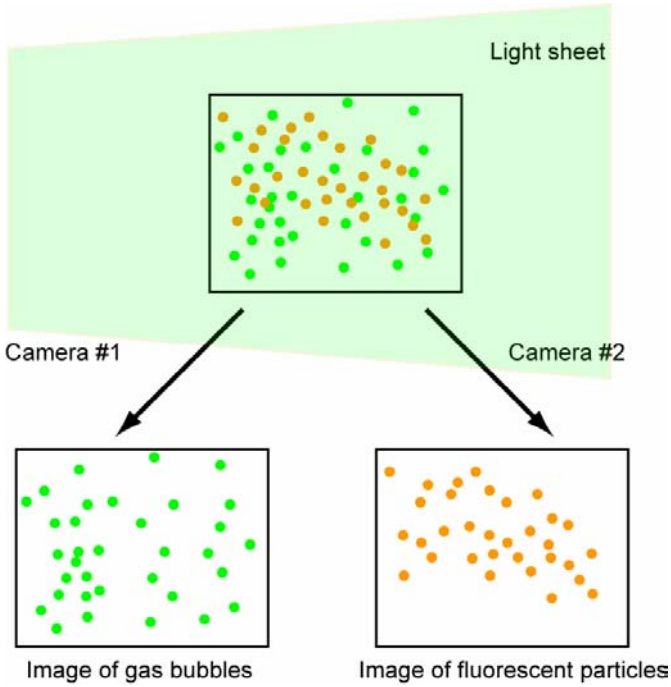

Figure 36: Combined PIV-LIF Provides Simultaneous Gas-Bubbles and Liquid Velocity Results.

6.0 EXAMPLES

6.1 Simultaneous Velocity Measurements and Cavitation Observation in a Radial Pump Impeller

Fig. 37 shows the top view of pump test rig for radial impeller pumps. The goal of this experiment is cavitation observation and their influence on the inlet flow of impeller. To get optical access for the two cameras a Plexiglas window in the pump casing is provided. In addition the shroud of the radial impeller has been also replaced by Plexiglas as well two of the impeller blades to ensure illumination. The two cameras are mounted side-by-side on a 3-axis-positioner, which also supports a mirror to deflect the image by 90 degrees. One camera is equipped with a low-pass filter to record the fluorescence images, the other is equipped with a band-pass filter, which enables simultaneous recording of cavitation images.

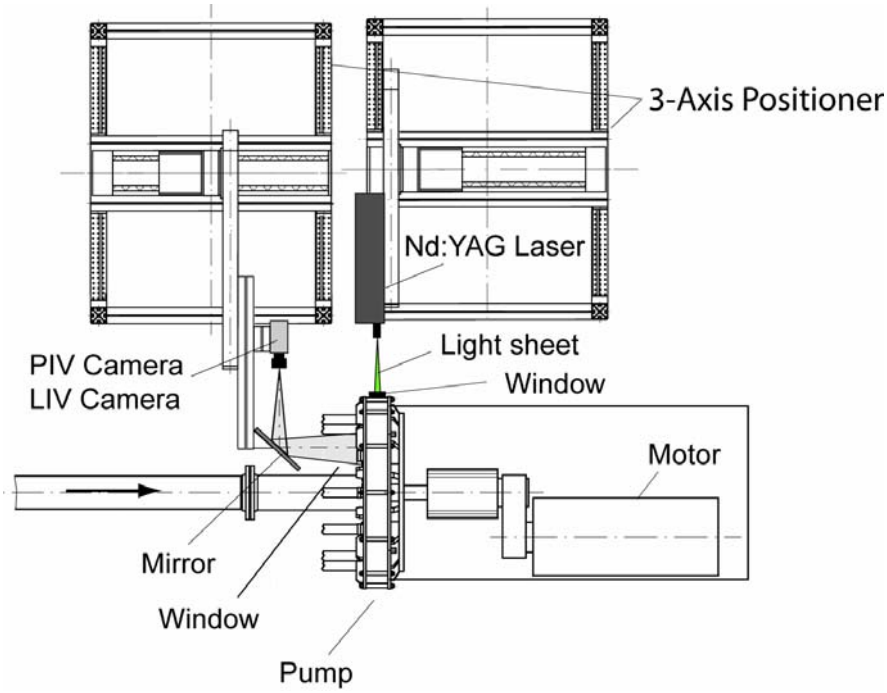

Figure 37: Test Rig for Combined PIV Measurements and Cavitation Observation.

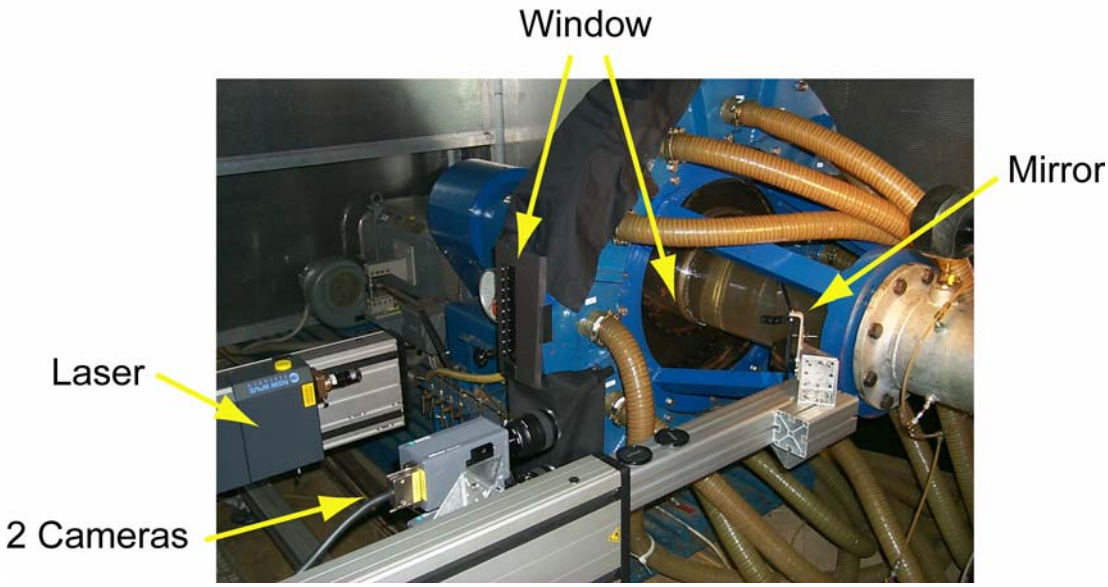

Figure 38: Picture of Test Rig for Combined PIV Measurements and Cavitation Observation.

Fig. 39 shows two simultaneous recorded images from the cavitating inlet flow of a radial impeller. The left image with the scattered light from the fluorescent particles will be used for PIV evaluation, while the right image is used for estimating the extent of cavitation. Fig. 40 compares two relative velocity maps, one measured with cavitation the other without.

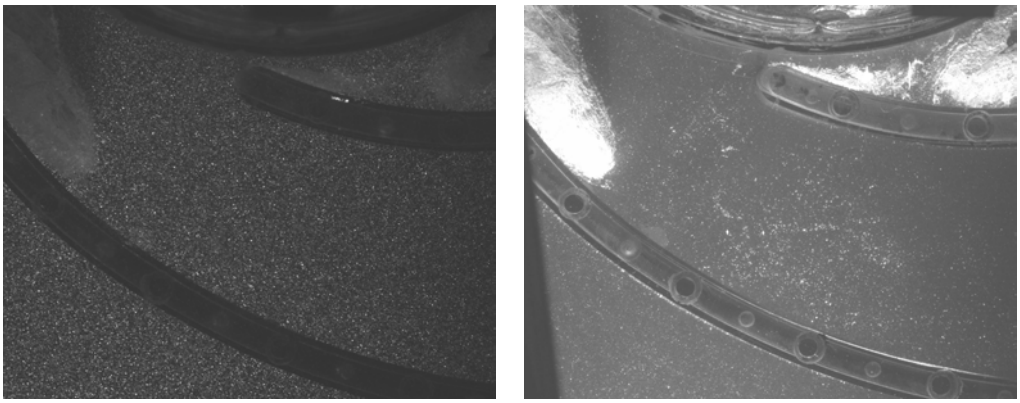

Figure 39: Pictures Taken at the Same Time with Different Filters. PIV Image (left) with Fluorescent Seeding, Cavitation Observation (right) [8].

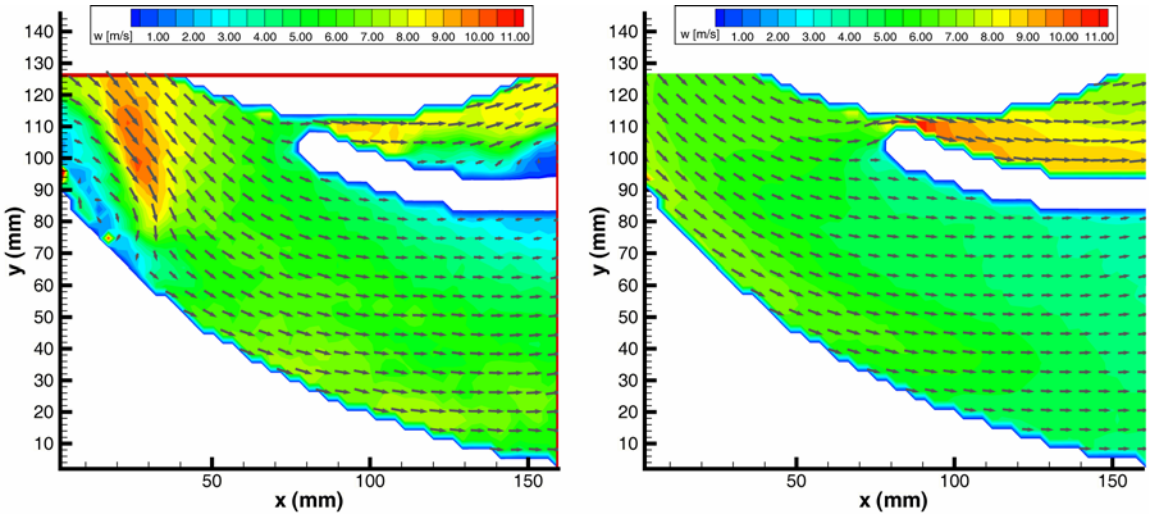

Figure 40: Relative Velocity in Radial Impeller With (left) and Without (right) Cavitation [8].

6.2 Mono and Stereo DPIV in Axial Flow Pump with Refraction Adaptation

Typically, there is an instable operating range in the performance curve of axial flow pumps at part-load. This is commonly attributed to stall inception and leads to a sudden decrease in pump head. As Fig. 41 shows this problem can be overcome by means of a simple but very effective casing treatment. This is achieved by machining shallow axial grooves in the casing wall ahead the rotor [9]. For PIV measurements a model of the axial flow pump with a Plexiglas casing was made. Using refraction matched SHELL GRAVEX oil unobstructed view for mono as well for stereo DPIV is ensured (Fig. 42 and Fig. 43). Refraction adaptation is so efficient that PIV measurements even with the grooved casing deliver good results. Major drawback in this experiment was the high viscosity of the fabrication oil used which affected the casing treatment. Fig. 44 shows one example of the mono DPIV measurements, which have been made according to the set-up II in Fig. 43. The velocity map illustrates the advantage of PIV to measure complex velocity fields since the recirculation on inlet of impeller is a highly unsteady process.

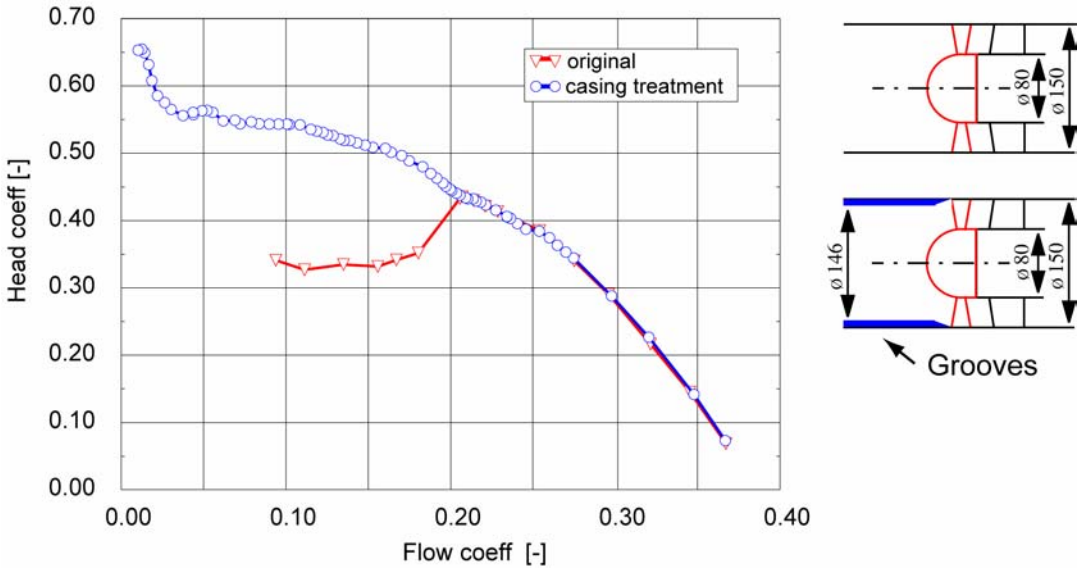

Figure 41: Axial Flow Pump Characteristics With and Without Casing Treatment.

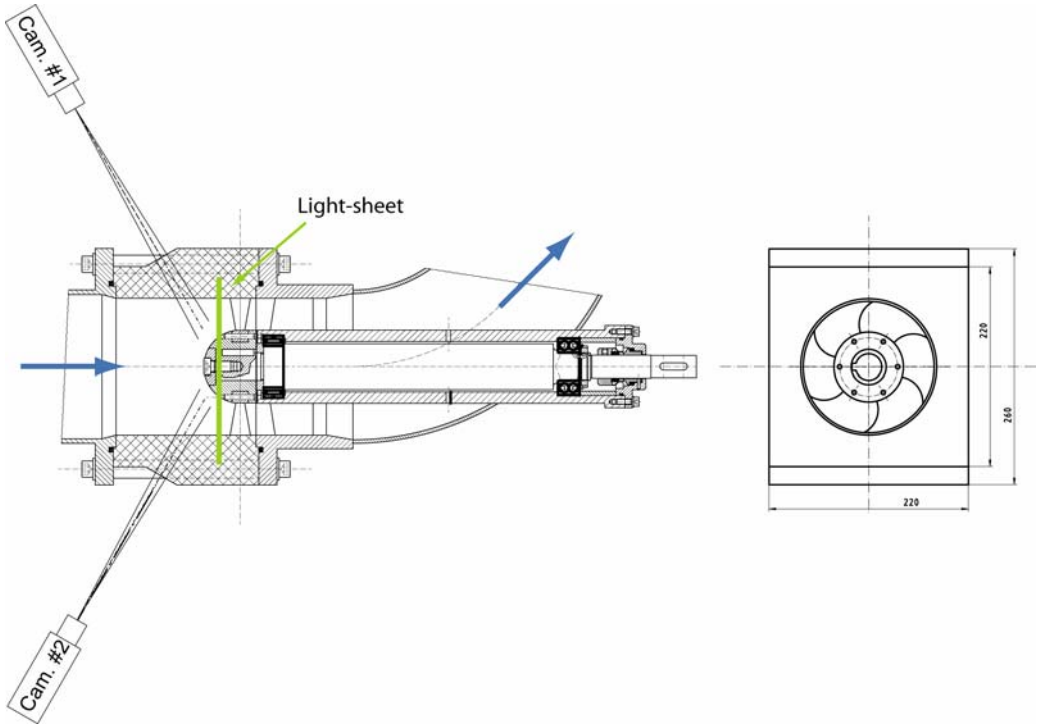

Figure 42: Stereo PIV with Diffraction Matched Fluid on an Axial Flow Pump (set-up I).

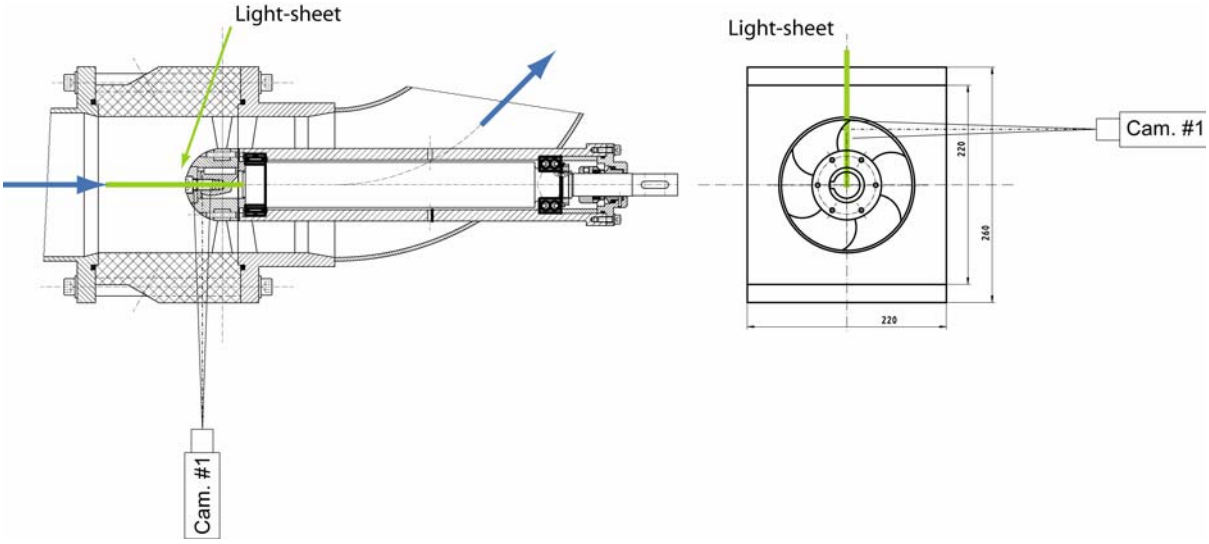

Figure 43: PIV with Diffraction Matched Fluid on an Axial Flow Pump (set-up II).

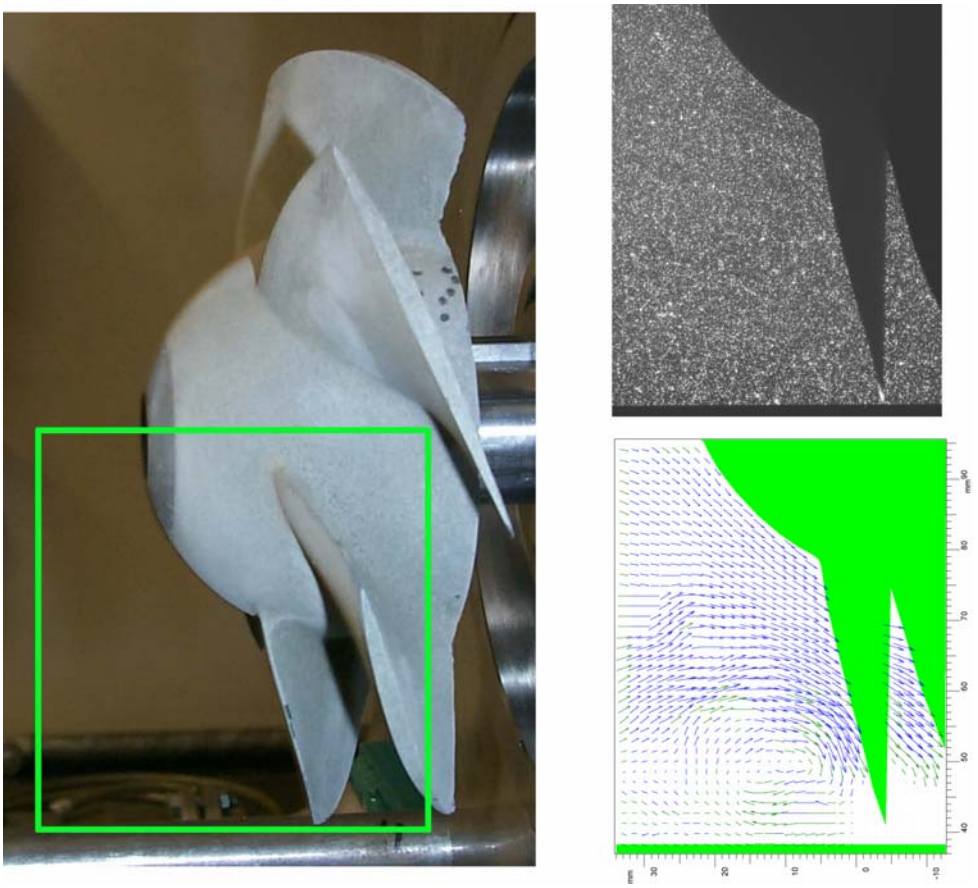

Figure 44: PIV Measurement of Recirculation on Inlet of Axial Flow Impeller (set-up II, Fig.).

6.3 Mono and Stereo DPIV in Axial Flow Pump

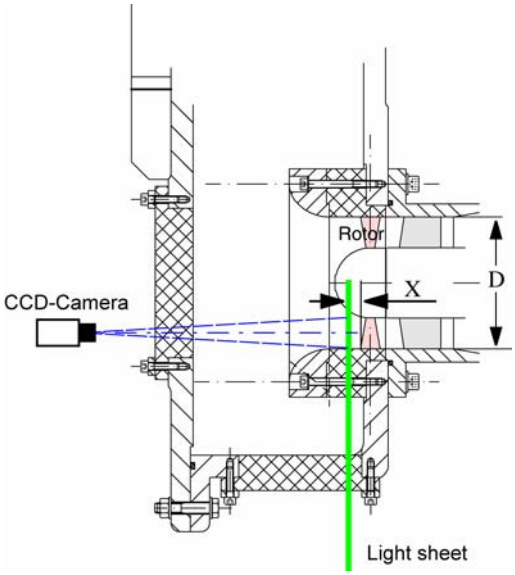

Figure 45: DPIV Measurements of Secondary Flow at the Inlet of an Axial Flow Pump.

Since viscosity has a major impact on the effect of casing treatment additional measurements with water as working fluid have been carried out. To get optical access a complete reconstruction of the pump was necessary. The suction pipe was replaced by an inlet chamber with flat windows. The set-up for stereo PIV illustrates Fig. 47. Two cameras each tilted by 30° allow measurement of three velocity components at the inlet plane. Distortion of the light sheet due to refraction was even with the grooved casing in an acceptable range. An additional window has been provided to ease the calibration process. Examples of the achieved results are shown in Fig. 46 and 48. Since the flow on part-load has a strong unsteady behaviour, phase averaged measurements are as well carried out.

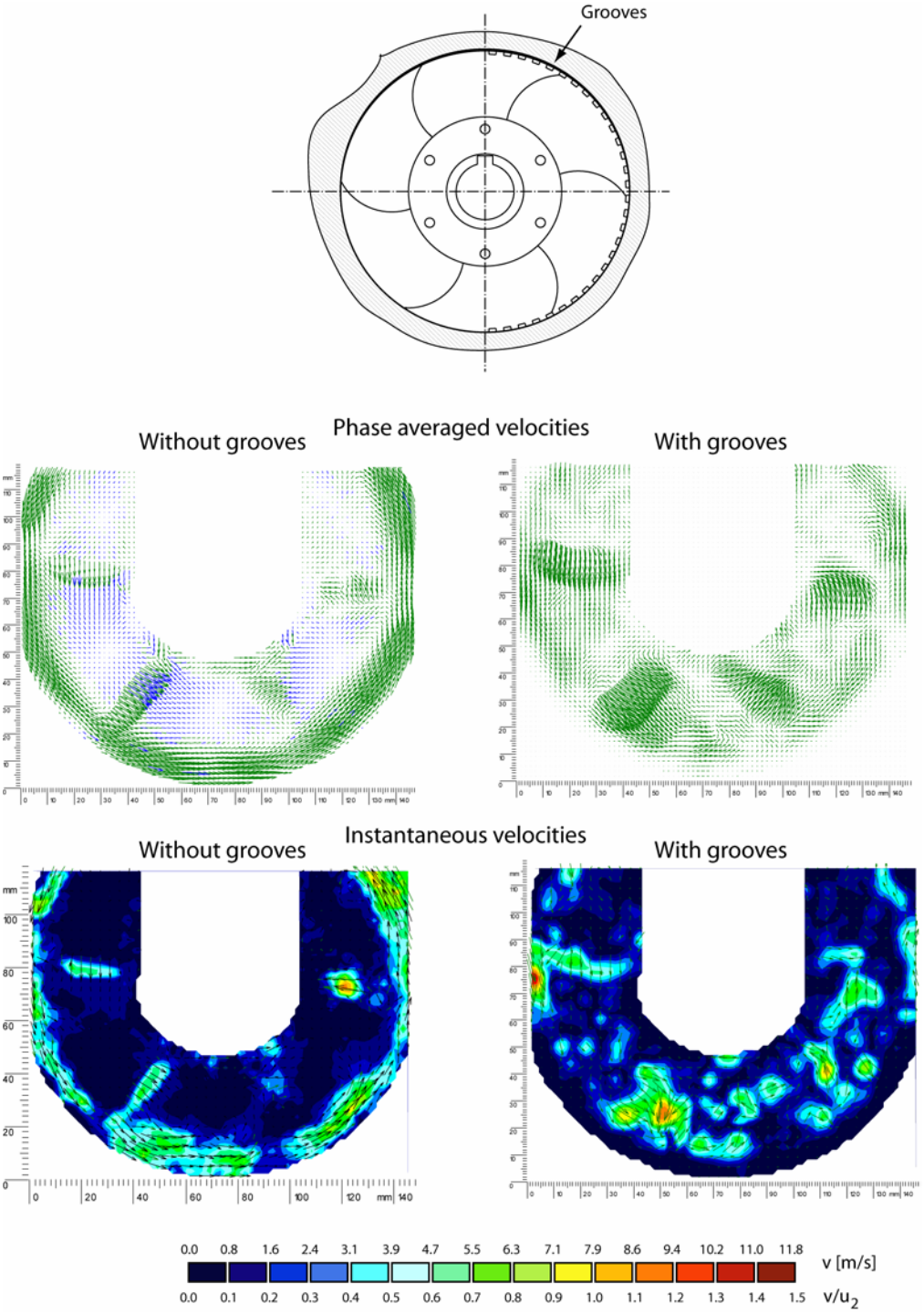

Figure 46: Circumferential Velocities on Impeller Inlet With and Without Casing Treatment.

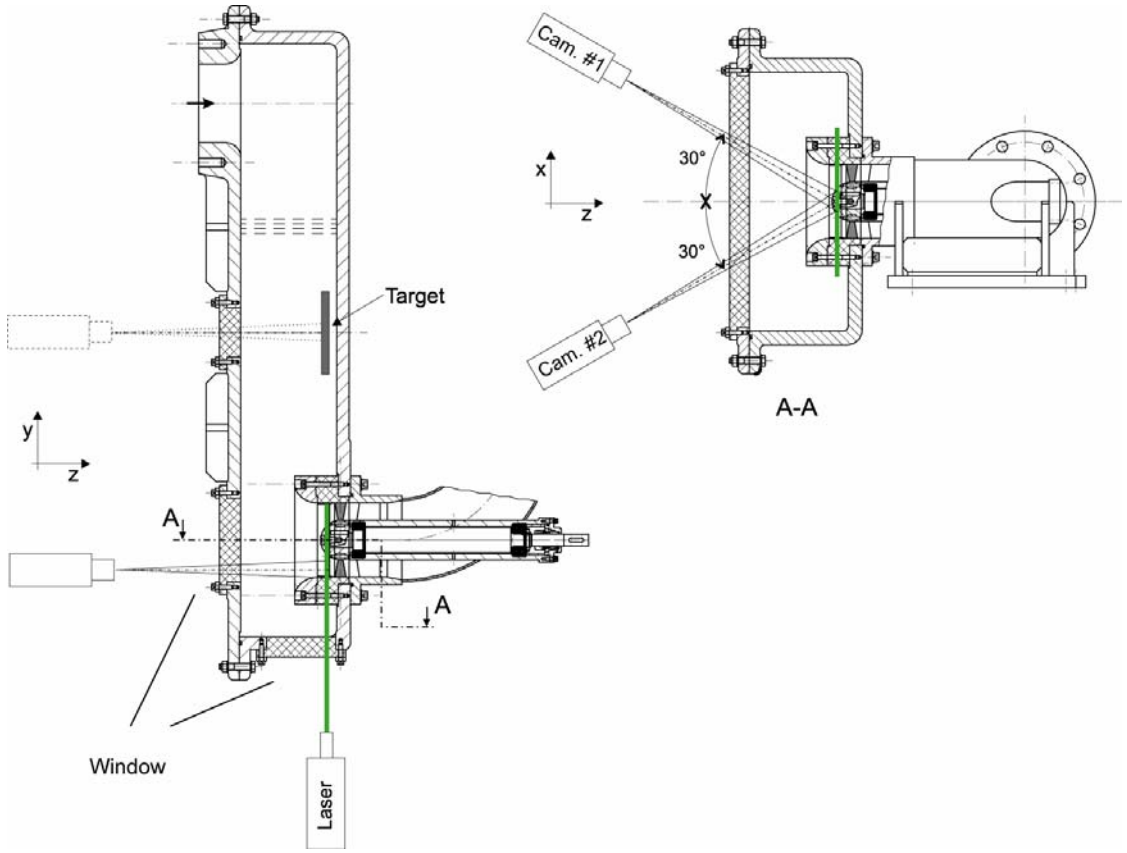

Figure 47: Stereo DPIV of Velocity at Inlet of an Axial Flow Impeller.

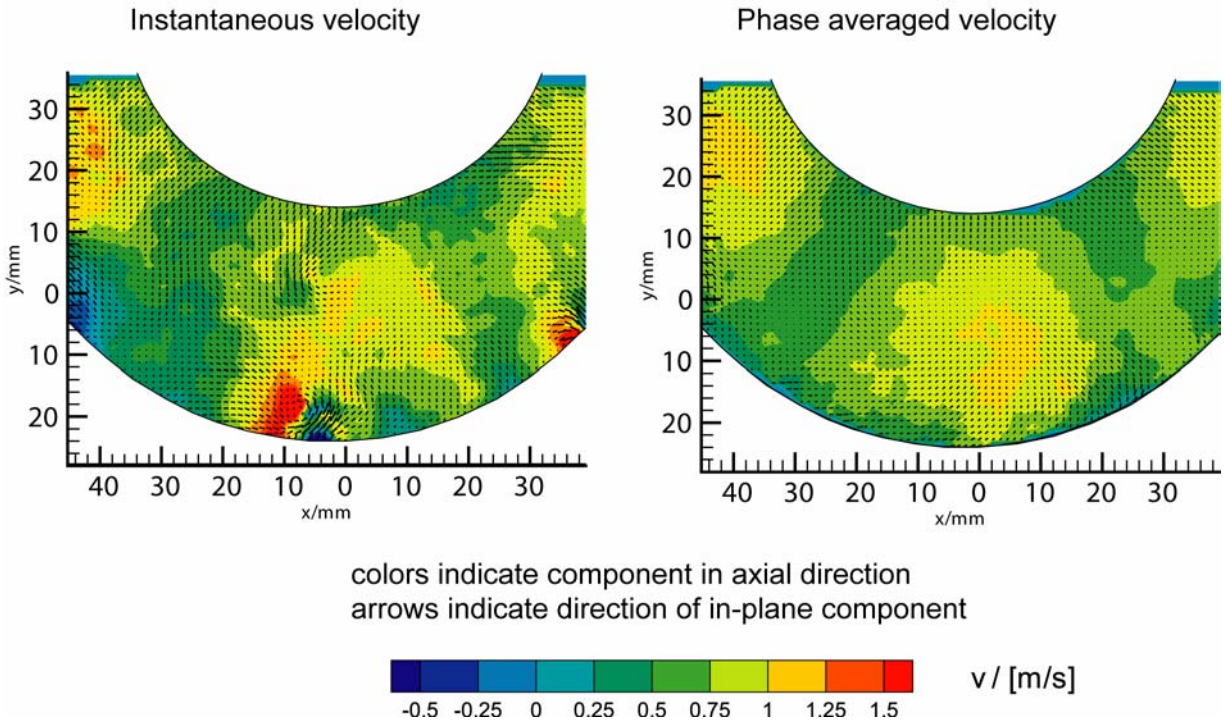

Figure 48: Results of Stereo DPIV at Inlet of an Axial Flow Impeller.

7.0 REFERENCES

[1] Adrian, R.J. (1995): *Limiting resolution of particle image velocimetry for turbulent flow*. Advances in Turbulence Research – 1995, Proc. 2nd Turbulence Research Assoc. Conf. Pohang Inst. Tech., pp. 1-19.

[2] Bates, C.J.; Sierra-Espinosa, F.Z.; O'Doherty, T.(1997): *A Comparison of DPIV and LDA Measurements in the Separated Region at the Branch Exit from a 90° Tee Junction*. Congress: Laser AnemometryAdvances and Applications. Karlsruhe 8.-11. September 1997, S. 117 bis 124.

[3] Bendat, J.S., Piersol, A.G. (2000). *Random Data*, 3rd ed. New York: Wiley.

[4] Brunn, A., Nitsche, W. (2000): *Analyse dynamischer Strömungsphänomene in überkritischen Diffusoren mit phasengemittelter PIV*. GALA e.V., 8. Fachtagung, 12.-14. Sept. 2000, Freising/ Weihenstephan.

[5] Chow, Y., Katz, J., Uzol, O., Meneveau, Ch. (2002): *An Investigation of Axial Turbomachinery Flows Using PIV in an Optically-Unobstructed Facility*. 9th Int. Symp. on Transport, Phenomena and Dynamics of Rotating Machinery, Honolulu, Hawaii, Feb. 10-14, 2002.

[6] Dantec Measurement Technology A/S (2000): *FlowMap. Particle Image Velocimetry Instrumentation*. 5th ed., August 2000, Skovlunde, Denmark.

[7] Dantec Measurement Technology A/S (2002): *FlowMap. 3D-PIV System*. 5th ed., 2002 Skovlunde, Denmark.

[8] Friedrichs, J. (2003). *Auswirkungen instationärer Kavitationsformen auf Förderhöhenabfall und Kennlinieninstabilität von Kreiselpumpen*. Mitteilungen des Pfleiderer-Instituts für Strömungsmaschinen, Heft 9, März 2003, 185 S., Dissertation TU Braunschweig 2003, Verlag und Bildarchiv W. H. Faragallah.

[9] Goltz, I., Kosyna, G., Wulff, D., Schrapp. H., Stark, U., Saathoff, H., Bross, S. (2004): *Structure of the Rotor Tip Flow in a Highly Loaded Single-Stage Axial-Flow Pump Approaching Stall. Part II: Stall Inception – Understanding the Mechanism and Overcoming its Negative Impacts*. ASME Heat Transfer/Fluids Engineering Summer Conference, July 11-15, 2004 Charlotte, NC, USA.

[10] Kramer, R.; Müller, H.; Mickan, B.; Dopheide, D. (1997): *LDA Extension for the Measurement of Radial Velocity Components in Piping Configurations*. Congress: Laser Anemometry Advances and Applications. Karlsruhe 8.-11. September 1997, S. 43 bis 50.

[11] Lai, W.T., Bjorkquist, D.C., Stefani, J. (1997): *Investigation of Flows in Rotating Machinery Using Particle Image Velocimetry*. 7th Int. Conference on Laser Anemometry, pp. 271-278. Advances and Applications, University of Karlsruhe, 8.-11. Sept. 1997.

[12] Melling, A. (1997): *Tracer particles and seeding for particle image velocimetry*. Meas. Sci. Technol. 8, pp. 1406-1416.

[13] Park, K.I., Bückner, Ch., Limberg, W.(1997): *Experimental Study of Velocity Fields in a Model of Human Nasal Cavity by DPIV*. Congress: Laser Anemometry Advances and Applications. Universität Karlsruhe 8.-11. September 1997, S. 617 bis 626.

[14] Pedersen, N. (2000): *Experimental Investigation of Flow Structures in a Centrifugal Pump Impeller using Particle Image Velocimetry*. Diss. 2000, ISBN 87-7475-239-1,Technical University of Denmark, Lyngby.

[15] Raffel, M., Willert, C., Kompenhans, J. (1998): *Particle Image Velocimtry*. Springer, Berlin.

[16] Schodl, R. (1986): *Laser-two-focus velocimetry*. AGARD-CP-399, paper 7.

[17] Uzol, O., Chow, Y.-C., Katz, J., Meneveau, C. (2002): *Unobstracted particle image velocimetry measurements within an axial turbo-pump using liquid and blades with matched refractive indices*. Experiments in Fluids 33, pp. 909-919.

[18] Stieglmeier, M., Tropea, C., Weiser, N., Nitsche, W. (1989): *Experimental Investigation of the Flow Through Axisymmetric Expansions*. Jour. of Fluids Engineering (111), pp. 464-471, ASME.

[19] Willert, C.E., Gharib, M. (1991): Digital particle image velocimetry. Experiments in Fluids 10 (193) 1991, pp. 181-193.

[20] Wernet, M.P. (2000): *Development of digital particle imaging velocimetry for use in turbomachinery*. Experiments in Fluids 28, 97-115, Springer.

[21] Westerweel, J. (1993): Digital Particle Image Velocimetry. Delft University Press.

[22] Westerweel, J. (1997): *Fundamentals of digital particle image velocimetry*. Meas. Sci. Technol. 8, pp. 1379-1392.

[23] Westerweel, J. (2005): Analysis of PIV interrogation with low pixel resolution. Proceedings of SPIE Volume: 2005 Optical Diagnostics in Fluid and Thermal Flow. pp. 624-635.

[24] Xiong, W.; Merzkirch, W. (1997): *DPIV experiments on turbulent pipe flow*. Congress: Laser Anemometry Advances and Applications. Karlsruhe 8.-11. September 1997, S. 475-482.